Review on CO_2 Activation via Catalytic Reverse Water-Gas Shift Reaction

Rafael Becka*, Siegfried Bajohr and Thomas Kolb

DOI: 10.1002/cite.70013

The reverse water-gas shift (RWGS) reaction offers a promising pathway for CO_2 utilization by converting CO_2 and H_2 into CO and H_2O. This review explores the thermodynamic challenges of the RWGS process, emphasizing the need for high temperatures to suppress side reactions such as methane and coke formation. For catalytic RWGS reaction, reaction mechanism and catalytic materials are discussed together with kinetic models to provide an insight into RWGS performance under varying conditions. Catalyst deactivation mechanisms, particularly metal sintering and coke deposition, are addressed, with strategies for enhancing catalyst longevity through material optimization. RWGS applications are discussed, demonstrating the potential for integrating RWGS into industrial settings.

Keywords: CO_2 activation, Reverse water-gas shift, Synthesis gas

Received: January 14, 2025; *revised:* June 30, 2025; *accepted:* July 01, 2025

1 Introduction

The effect of human-induced climate change, such as rising sea levels, more frequent and intense extreme weather events, and changing ecosystems, are some of the main challenges of the current and future generation [1, 2]. The constant rise of global greenhouse gas concentrations, driven by emission of carbon dioxide (CO_2) and other greenhouse gases, is linked to the combustion of fossil fuels as well as their use in industrial processes [1]. While many CO_2 sources can be eliminated by rigorous electrification, e.g., in the energy and mobility sector [3], decarbonizations may not be practicable for a large number of industrial processes.

This is particularly true for the chemical industry, which accounts for approximately 5 % of global greenhouse gas emissions. Carbon-based educts are essential in this sector because they serve as feedstock for carbon-based products, resulting in unavoidable CO_2 emissions [4]. Since carbon and CO_2 cannot be entirely avoided in these processes, recycling them within a circular economy is crucial to achieve a climate-neutral society by 2050, as envisioned by the European Green Deal [5].

The catalytic reverse water-gas shift (RWGS) reaction, which converts CO_2 and H_2 into CO and the by-product H_2O as described in Eq. (1), holds significant promise for a sustainable chemical industry. This reaction provides a crucial link between carbon capture and utilization (CCU), green hydrogen production by water electrolysis, and well-known processes based on synthesis gas to produce basic chemicals such as methanol and acetic acid as well as potential substitutes for fossil fuels via Fischer-Tropsch synthesis as illustrated in Fig. 1 [6].

$$CO_2 + H_2 \rightleftharpoons CO + H_2O; \quad \Delta_R H^0 = 42.1\ \mathrm{kJ \cdot mol^{-1}} \qquad (1)$$

CO_2 is significantly more stable than CO, being the highest oxidation state of carbon and therefore possessing the lowest energy level [7]. This results in a high energy demand to convert CO_2 into other molecules (activation energy). The required energy can either be supplied by other high-energetic reactants such as H_2 or through external sources, e.g., thermal energy, electricity or light [8]. However, in processes like the phosgene synthesis or acetic acid production, hydrogen as a chemical energy carrier is not involved and reaction temperatures are too low for thermal activation of CO_2 [9, 10]. Consequently, CO_2 has to be activated in a separate step, e.g., via RWGS reaction, before it can be used as a feedstock for these synthesis reactions. For other processes, e.g., Fischer-Tropsch synthesis, the deployed catalysts are not suitable for a direct use of CO_2 as reactant.

Some processes can utilize CO_2 and H_2 directly as a feedstock – for instance, methanol synthesis [11] or methanation via the Sabatier reaction [12] – but the upstream activation

[1]Rafael Becka https://orcid.org/0009-0002-0925-1394 (Rafael.Becka@kit.edu), [1]Dr.Ing. Siegfried Bajohr, [1]Prof.Dr.-Ing. Thomas Kolb
[1]Karlsruher Institute of Technology - KIT, Engler-Bunte-Institut Fuel Technology, Engler-Bunte-Ring 1, 76131 Karlsruhe, Germany.

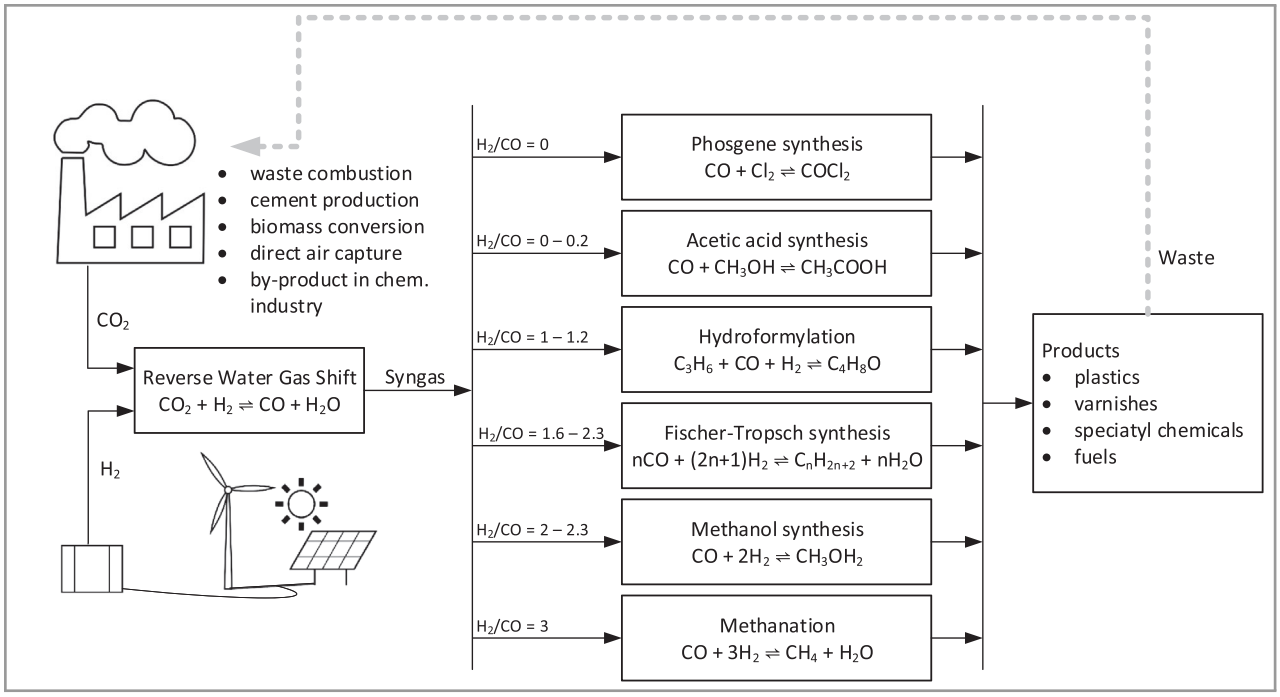

Figure 1. Reverse water-gas shift as a link between carbon capture and basic chemical industry based on [6].

of CO_2 into CO offers several advantages. When methanol or methane are synthesized from CO hydration instead of CO_2 hydration, less water is produced. This leads to a more favorable equilibrium composition according to Le Chatelier's principle [13], and an increased reaction rate due to the higher reactivity of the CO molecule compared to CO_2 [14]. Moreover, in methanol synthesis, the presence of H_2O as a byproduct when using a CO_2-based feedstock is known to accelerate catalyst deactivation, thereby reducing catalyst lifetime [15–18]. Therefore, the implementation of RWGS and water separation before the respective synthesis reaction could be advantageous compared to the direct synthesis using CO_2.

Converting CO_2 and H_2 into synthesis gas also offers practical advantages for introducing renewable feedstocks into established industries. Already existing plants that are designed for conventional synthesis gas and large-scale operation can continue to be operated either by fully substituting fossil fuel-based synthesis gas with CO_2- and H_2-derived synthesis gas or through partial integration. Such approaches minimize the initial investment required for new plants, making the transition more economically viable.

Today, the RWGS reaction is primarily utilized and well-established in the reverse direction, namely, towards CO_2 and H_2 (water-gas shift; WGS). In this case, the main purpose is to increase the hydrogen content in synthesis gas production to adjust the stoichiometric H_2-to-CO/CO_2 ratio to suit subsequent synthesis processes [19, 20]. Examination of the reaction conditions of the RWGS and the WGS reveals a notable difference in the temperatures that need to be applied for the different processes. RWGS is more favorable at high temperatures due to its endothermic nature [14], whereas WGS is thermodynamically preferred at lower temperatures [20]. This disparity highlights the limited applicability of well-established knowledge from WGS to RWGS. For this reason, this review paper aims to provide an overview of the current scientific investigations in literature in the area of thermodynamics, catalysts, reaction kinetics, and the technological readiness of various RWGS implementation approaches across different scales.

Although this review focuses on catalytic RWGS, it is important to note that significant research efforts are being directed towards alternative process routes. These include thermal RWGS, plasma RWGS, solar-induced RWGS, and biological RWGS. For more information on these alternative approaches, readers are referred to the available literature [14, 21–24].

2 Theoretical Background and Thermodynamics of the RWGS Reaction

When considering a gas mixture of the reacting components in Eq. (1), it becomes evident that the RWGS reaction is not the only possible reaction, depending on the applied temperature. Other possible reactions include the methanation of CO_2 (Sabatier reaction) and CO into methane (CH_4). Once CH_4 is involved in the reaction system, the

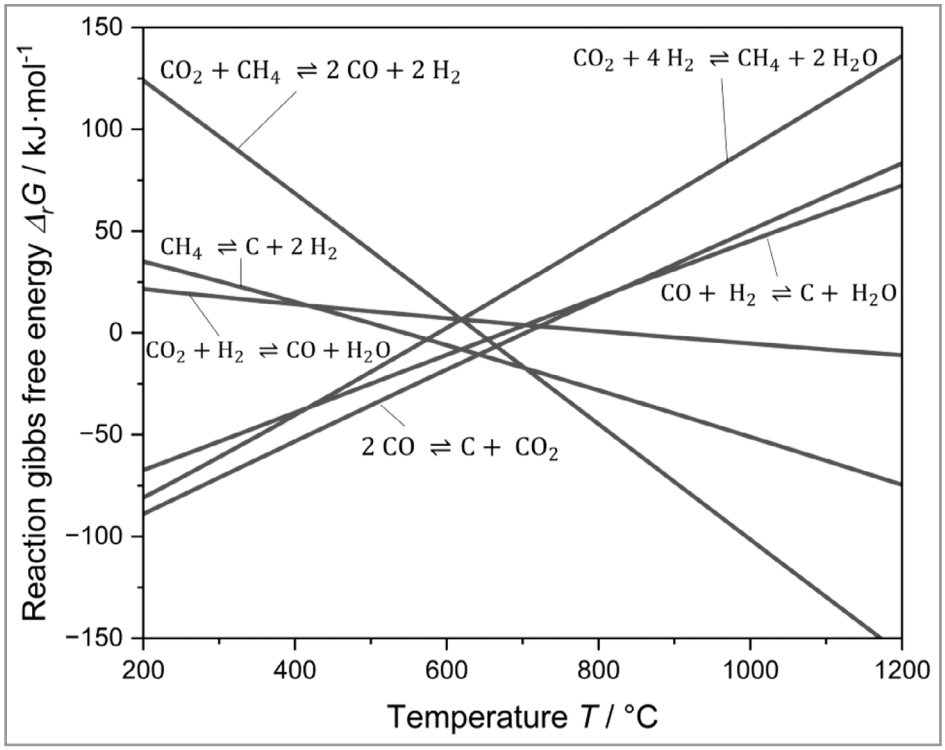

Figure 2. Reaction Gibbs free energy for selected reaction under RWGS conditions with equimolar ratio of CO_2 and H_2.

dry reforming reaction may also occur, where CO_2 and CH_4 react to form CO and H_2. Since RWGS reaction implementations typically involve elevated temperatures, coke (C) formation must also be considered. Coke can be produced from the pyrolysis of CH_4, as well as from the reverse heterogeneous WGS reaction, in which CO and H_2 react to solid carbon and H_2O. Additionally, coke formation can occur through the Boudouard reaction, where CO disproportionates into C and CO_2, and the Bosch reaction, where coke is formed from CO_2 and hydrogen. These competing reactions, particularly at high temperatures, underscore the complexity of the RWGS reaction systems [25, 26].

Fig. 2 illustrates the change in Gibbs free energy (reaction Gibbs free energy, $\Delta_R G$) for some of the previously mentioned reactions as a function of reaction temperature, calculated using the non-random two-liquid (NRTL) equation-of-state in Aspen plus [27]. Reactions not included in Fig. 2 are the steam reforming reaction, the Bosch reaction, and the reverse gasification reaction. The first two are omitted because they represent a combination of other depicted reactions (CO_2 hydration and reverse heterogeneous WGS) with the RWGS reaction. The reverse gasification reaction is excluded due to its significantly higher order of magnitude in the reaction Gibbs free energy, making its occurrence unlikely compared to the other reactions.

The Gibbs free energy G is a variable of state, describing the thermodynamic potential of a system according to Eq. (2) [28]. It depends on the system temperature T, system pressure p, the composition $\{N_i\}$, and the system entropy S [29]. The change in Gibbs free energy, $\Delta_R G$, therefore provides a prediction of the thermodynamic favorability of a chemical reaction and is directly linked with the chemical equilibrium constant, K_{eq}, via Eq. (3), with the universal gas constant R and the reaction temperature T. For reactions where the change in Gibbs free energy value is less than zero, the total entropy of the system in a stoichiometric ratio increases, resulting in a spontaneous reaction without the need for external energy input [27, 28].

$$G\,(T,\,p,\,\{N_i\}) = H(T,\,p,\,\{N_i\}) - TS \tag{2}$$

$$K_{eq} = e^{\frac{-\Delta_R G}{R \cdot T}} \tag{3}$$

The Gibbs free energy for the stoichiometric RWGS reaction becomes negative only at temperatures above 800 °C. This indicates that for efficient CO production from CO_2 either high temperatures or a high hydrogen concentration must be applied, as dictated by Le Chatelier's principle [29]. Furthermore, the change of the Gibbs free energy of the RWGS reaction exhibits only a minor negative gradient, suggesting that raising the temperature has a limited effect of increasing the equilibrium concentration of the desired product CO.

By-products such as methane and coke must also be considered. Methane can be produced through the hydrogenation of CO and CO_2. Although both reactions have a positive Gibbs free energy at the elevated temperatures required for efficient RWGS, large concentrations of CO and CO_2, combined with abundant H_2, drive the chemical

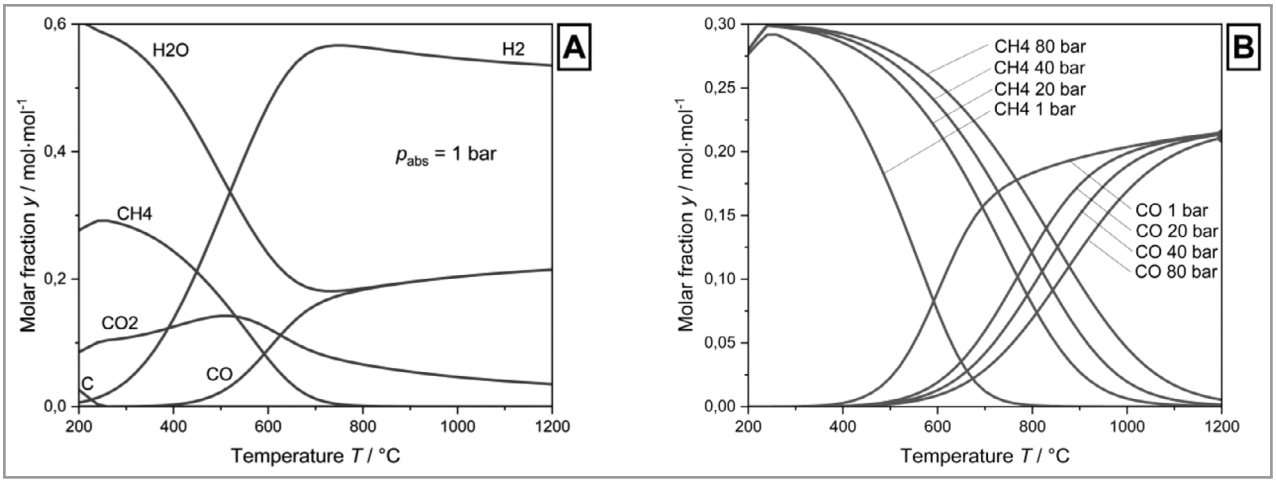

Figure 3. Equilibrium composition for different temperatures (A) and (absolute) pressures (B) for a feed CO_2 to H_2 molar ratio of 1:3.

equilibrium towards methane formation. This effect is further amplified under elevated pressure, which may be necessary for downstream synthesis reactions and achieving feasible plant sizes [13, 29].

Similarly, the Boudouard reaction and the reverse heterogeneous WGS reaction can lead to coke formation from CO. Despite their positive Gibbs free energy, high concentrations of CO/H_2 and elevated pressure can promote coke formation. Additionally, once methane is present in the system, coke formation via methane pyrolysis becomes possible, as this reaction has a negative Gibbs free energy at reaction temperatures of $T > 500$ °C.

Coke formation is generally undesirable in catalytic processes as it reduces the active surface area of the catalysts, causes blockages inside the reactor and downstream equipment, and leads to metal dusting corrosion [30]. Metal dusting corrosion involves the formation of metal carbides (M_3C) through the interaction of metals with carbon on metal surfaces. These carbides diffuse to the graphite surface and detach, causing irreversible material degradation, even if the graphite is removed regularly [31].

While coke formation via methane pyrolysis can be mitigated by suppressing methane formation through high reaction temperatures [32], coke formation from the Boudouard reaction and the reverse heterogeneous WGS reaction can potentially be suppressed by a high surplus of CO_2, promoting the Boudouard reaction towards CO or a high concentration of H_2O to promote the heterogeneous WGS reaction (steaming). However, both strategies pose challenges for RWGS efficiency. Most of the CO_2 is desired to convert into CO and H_2O shifts the chemical equilibrium of the RWGS reaction back towards CO_2.

Fig. 3A shows the calculated equilibrium composition based on the Gibbs free energy for a feed with a CO_2-to-H_2 molar ratio of 1:3. This ratio is representative of conditions typically used for subsequent processes such as methanol synthesis or Fischer-Tropsch synthesis.

It can be observed that even at ambient pressure a temperature above 800 °C is necessary to completely suppress CH_4 in chemical equilibrium. At temperatures exceeding 800 °C a further increase in temperature has only a limited effect on the CO-to-CO_2 ratio as indicated by the reaction Gibbs free energy in Fig. 2. The reachable CO_2 conversion in equilibrium at ambient pressure is therefore limited to about 80 % meaning a CO molar fraction of 20 % in equilibrium. The notable amount of coke below 250 °C is assigned to Boudouard reaction and heterogeneous WGS reaction that have negative reaction Gibbs free energy.

Fig. 3B illustrates the impact of reaction pressure on CO and CH_4 concentration in chemical equilibrium for a CO_2-to-H_2 molar ratio of 1:3. According to Le Chatelier's principle, the mole-reducing CO_2 hydration reaction benefits from an increased system pressure, which reduces the amount of CO_2 and H_2 available for conversion into CO and H_2O via the RWGS reaction. Consequently, CO_2 conversion to CO decreases as pressure increases, even though the RWGS reaction itself is unaffected by pressure because the number of molecules remains constant throughout the reaction. As mentioned before, when CH_4 is present at temperatures above 500 °C, negative reaction Gibbs free energy for methane pyrolysis indicates coke formation. Consequently, the reaction temperature has to be significantly higher than 800 °C for RWGS under pressure.

Coke formation during the RWGS reaction can be mitigated at high temperatures; however, it remains an undesired side reaction when the CO-containing product gas is cooled down for downstream processes. At temperatures below 650 °C, the Gibbs free energy of the heterogeneous WGS reaction and the Boudouard reaction becomes negative, promoting coke formation. This can result in heat exchanger blockages and a subsequent pressure increase [33, 34]. To prevent coke formation during the gas cooling process, the temperature must be reduced rapidly. However, this rapid cooling poses challenges for efficient heat recovery.

In conclusion, temperature is a critical parameter of the RWGS reaction – not primarily to boost the RWGS reaction but to suppress methane and coke formation. This becomes even more pronounced at elevated reaction pressures, which may be necessary for downstream processes. As an example, at a pressure of 20 bar, that would be suitable for subsequent Fischer-Tropsch synthesis, reaction temperature must exceed 1100 °C. To achieve this temperature, a high energy input is necessary that can be supplied thermally by partial combustion of hydrogen [35] or electrically, e.g., in plasma RWGS [36]. Another approach is the introduction of CO_2 and H_2 into other high-temperature processes such as partial CH_4 oxidation, as investigated in the Scoore project [37].

A process option considered more frequently is the catalytic RWGS reaction. Specific reactions can be promoted or suppressed based on their activation energy, which acts as a kinetic barrier. This barrier is determined by the reaction mechanism, which can be influenced or modified through the use of different catalytic materials [15, 20]. Suppressing CH_4 formation at low temperatures allows for more CO_2 to remain available for conversion into CO. In this case, a highly active and selective catalyst can enable a high CO yield at temperatures significantly lower than 800 °C. Thus, beyond chemical equilibrium considerations, the reaction mechanism and reaction kinetics of the catalyzed RWGS are critical for determining optimal reaction conditions and the achievable product composition. In addition to product composition, operating the RWGS reaction with a catalyst at lower temperatures offers several advantages by lowering the energy input that is necessary to reach the desired product composition and lowering the equipment costs. High reaction temperatures in contrast present challenges for the catalyst, as catalyst activity tends to decline over time due to deactivation processes such as catalyst sintering and phase separation [38–40].

3 Reaction Kinetics and Catalysts for Reverse Water-Gas Shift

The performance of catalytic CO_2 activation via RWGS relies heavily on the choice of the catalytic material. It determines the dominant reaction mechanism and reaction kinetics as well as optimal reaction conditions and achievable product composition. This chapter presents possible mechanisms of CO_2 activation on catalytic surfaces, detailing the adsorption processes, reaction pathways, and subsequent desorption of intermediates. A comprehensive exploration of catalyst materials and their modifications is provided, aiming to enhance selectivity, efficiency, and stability of the active material. Furthermore, the chapter addresses reaction kinetic models and catalyst stability, offering insights into the long-term performance and degradation mechanisms of catalytic systems for RWGS reaction.

For the comparison of different catalysts for RWGS, two measures are used: CO_2 conversion X_{CO2} that describes the number of moles of CO_2, n_{CO2}, that remain after the reaction with respect to the initial amount of moles of CO_2, $n_{CO2,\,0}$, as described in Eq. (4), and CO selectivity, S_{CO}, according to Eq. (5), which describes the number of moles of CO that are formed during the reaction, $(n_{CO} - n_{CO,0})$, compared to the total amount of CO_2 that has been converted into product molecules, $(n_{CO2,0} - n_{CO2})$.

$$X_{CO_2} = \frac{n_{CO_2,0} - n_{CO_2}}{n_{CO_2,0}} \tag{4}$$

$$S_{CO} = \frac{n_{CO} - n_{CO,0}}{n_{CO_2,0} - n_{CO_2}} \tag{5}$$

3.1 RWGS Reaction Mechanism

The first step of CO_2 activation via catalyzed RWGS is the adsorption of CO_2 onto the catalytic surface. Chemisorption is considered the dominant adsorption mechanism at relevant temperatures (>25 °C) [41]. Since the CO_2 molecule consists of two oxygen atoms with lone pairs of electrons and one carbon atom without lone electrons, there are three possible adsorption structures on the catalyst surface, as illustrated in Fig. 4.

1. Oxygen as an electron donor: The oxygen atoms can donate electrons to an electrophilic Lewis acid site on one or two active centers (Fig. 4C and Fig. 4D illustrate adsorption on two active centers).
2. Carbon as an electron acceptor: The carbon atom can accept electrons from a nucleophilic Lewis base site on a single active center (Fig. 4A).
3. Mixed coordination: A combination of oxygen-donating and carbon-accepting electrons is also possible, either on one or two active centers (Fig. 4B illustrates adsorption on two active centers).

In addition to the direct adsorption on an active surface site, the CO_2 molecule can also interact with surface hydrogen bonds, free hydrogen ions, or a surface hydroxyl group to form a surface carbonate [22, 23]. During adsorption, the linear CO_2 molecule bends due to strong valence forces, which lowers the electron acceptance barrier and enables the subsequent surface reaction steps [22, 42].

After adsorption of the CO_2 molecule, that is considered the rate-determining step [43], there are two accepted theories for the kinetic mechanism of CO_2 conversion into CO via RWGS as indicated in Fig. 4.

1. Direct dissociation of the CO_2 molecule on the surface of a catalytic material via a redox mechanism. For direct dissociation, it is assumed that the CO_2 molecule is reduced by an electron donor on the surface (metal or oxygen vacancy). The CO molecule is released and in a second step the oxidized active center is reduced by hydrogen to its initial state [44–46].

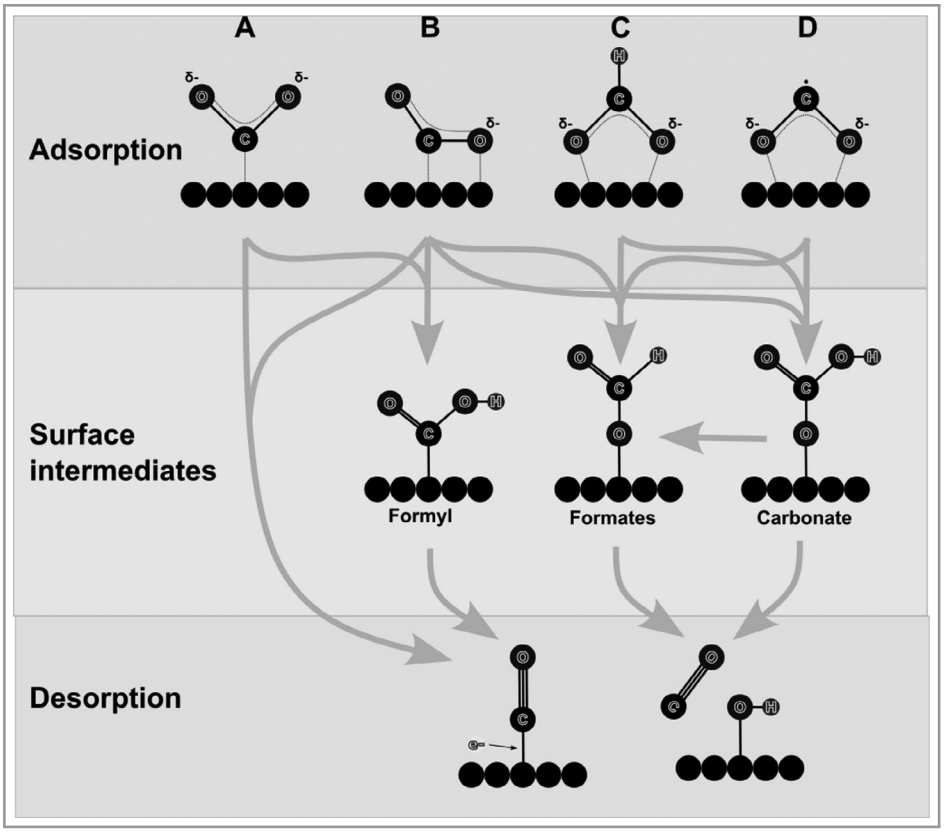

Figure 4. Proposed reaction mechanism for RWGS reaction: Adsorption structures, surface intermediates, and desorption based on [44–46].

2. H_2-mediated dissociation where CO_2 forms a surface intermediate containing hydrogen [14]. When hydrogen is directly involved in the CO_2 dissociation, a surface intermediate is formed. Depending on the catalyst material and the reaction conditions, different reaction paths can be considered. In the formates reaction route, one oxygen atom acts as an electron donor to the active site while donates electrons to the carbon atom, forming formic acid. Hydrogen then recombines with adsorbed oxygen to form a surface hydroxyl group, and CO is released. Another possible reaction pathway is the formation of formyl. In this case, the carbon atom is directly linked to the surface and acts as an electron acceptor. Additionally, carbonates can be formed as surface intermediates that are sequentially disassembled to formates and eventually CO [44–46].

Both mechanisms (direct dissociation and H_2-mediated dissociation) are observed across different catalytic materials to varying extents [47–52]. For the H_2-mediated dissociation, the formyl route is typically the primary pathway considered [46]. Although formate species have been detected on various catalytic surfaces [53], they are often considered to act as a spectator species due to their high stability [54–57]. The dominance of either direct dissociation or H_2-mediated dissociation depends on several factors: the oxygen affinity of the catalytic material, the crystallite properties, the reaction conditions, and the oxygen and hydrogen coverage of the active surface [46].

The reaction mechanism described for the H_2-mediated RWGS reaction path is identical to the initial reaction steps proposed for methanation and methanol synthesis from CO_2 [22, 58, 59], that employ similar catalyst materials. It is unsurprising that catalysts promoting the H_2-mediated reaction path over direct dissociation tend to exhibit higher selectivity towards CH_4 than materials favoring the direct dissociation mechanism [60–62]. Other synthesis routes, such as those producing ethanol, ethylene, ethylene glycol, and various aldehydes, are assumed to begin with adsorbed CO species [22]. This poses two significant challenges for the RWGS reaction: firstly, the desired product is used to form a byproduct resulting in a decrease in selectivity, and secondly, the formation of a byproduct is effectively blocking active centers for CO production, resulting in a decrease in conversion rate. For instance, Qi et al. [52] demonstrated that methanation is energetically favorable on all metals that have been studied. Methanation not only blocks active sites required for H_2-mediated dissociation of CO_2 to CO but also competes for active sites involved in direct dissociation on Pt, Pd, Co, Fe, Ru, and Rh.

A potential solution to increase CO selectivity involves minimizing the contact time between catalyst and the reacting gas [63–66]. This approach forces multiple reactant

Table 1. Proposed sequences of catalyst activity of different materials from high to low activity for RWGS reaction.

Catalyst activity	Method	Source
Rh > Ni > Pt > Pd > Cu > Ag	DFT study	[46]
Rh, Ni > Pt, Pd > Cu > Co > Ru > Fe	DFT study with microkinetic modeling	[52]
Pt > Pd > Ni > Fe, Cu	Experimental investigation, electric field-assisted	[78]
Ni > Cu > Co > Fe	Experimental investigation	[79]
Cu > Co	Experimental investigation	[80]

molecules to compete for a limited number of active sites, promoting the desorption of formed CO. Similarly, loading only small amounts of active metal onto the catalyst carrier achieves the same effect. Ranjbar et al. [67] compared different Ni-loadings in a MgO carrier and found that the selectivity towards CO almost reaches 100 % for a 2 % Ni load on MgO compared to around 50 % CO selectivity for a 15 % Ni loading at 400 °C. The same effect was observed for TiO_2-supported Rh catalysts [68]. However, both strategies, namely, short contact times and low metal loadings, come with the drawback of reduced CO_2 conversion, decreasing the RWGS reaction efficiency [64, 67].

The size of metal crystals on the support material also affects CO selectivity. Larger crystal diameters favor CH_4 production [69–71], while smaller crystals enhance CO selectivity [68]. This may be because CH_4 formation requires more surface hydrogen than CO formation, and larger structures provide more active sites for hydrogen dissociation.

To achieve both high CO selectivity and efficient CO_2 conversion, research is focusing on optimizing the active material, support structure, and doping elements. The aim is to develop catalysts that balance these competing factors to improve overall performance.

3.2 Catalyst Materials for RWGS

Many materials have been identified to catalyze the RWGS reaction, including Pt, Pd, Au, Cu, Co, Rh, Ru, Ni, Mo, and Fe. Current research on catalytic material focuses on combining these metals with support materials, doping agents, and multi-metal systems [72], as well as optimal catalyst loadings and metal crystal sizes [70]. Since this review aims to provide a condensed overview of critical aspects of the RWGS reaction, a detailed overview of recent studies is not included here. Instead, general trends in catalytic systems will be highlighted. For comprehensive reviews on catalyst development the readers are referred to available literature [14, 24, 72, 73].

For the pure active material in crystallite form, various working groups have proposed different rankings for the catalyst activity, summarized in Tab. 1. Although there are some inconsistencies, the general order can be identified to Rh and Ni as the most active catalyst materials, Pt, Pd, Cu, Co as intermediate active catalysts, and Fe and Ag with lower catalytic activity. In addition to transition metals, certain metal carbides, such as Mo2C [74–76] and WC [77] also exhibit catalytic activity for RWGS reaction.

The order of catalytic activity presented in Tab. 1 can be linked to the interaction between the catalyst material and the oxygen atom of the adsorbed CO_2. As previously discussed, this interaction influences the extent to which CO_2 is dissociated directly or via H_2 mediation. It also affects the activation energy of dissociation and, consequently, the activity of the catalyst. Dietz et al. [46] observed that the commonly reported catalytic activity order correlates with the oxygen affinity of the catalyst material (Ni < Rh < Cu < Pd < Pt < Au). This finding suggests that direct dissociation of CO_2 into CO is advantageous for achieving a high catalyst activity and CO selectivity. Therefore, doping and support material should be chosen to enhance the oxygen affinity of the catalyst material.

Catalyst doping involves incorporation of hetero-atoms (promoters) into the host lattice of a catalytic material to enhance its activity, selectivity, and stability [81]. Two different types of catalyst doping can be differentiated: alkali (metal) doping and doping with another transition metal to form a bimetallic catalyst [14].

3.2.1 Bimetallic Catalysts

One of the most studied bimetallic catalysts is ZnO-doped Cu, which is also widely used in methanol synthesis. ZnO doping has been shown to increase the dispersion of Cu on the carrier material and stabilize the catalyst surface during reaction [82]. Regarding hydrogen, ZnO is assumed to be hydrated and hydroxylated through interaction with spilt hydrogen. This results in a mobile ZnO-hydroxyl species that enhances copper activation and catalyst activity [83]. The activity of a Pt/Co bimetallic catalyst exhibits the activity of both Pt and Co catalyst, while the selectivity slightly decreases [84]. Similar synergetic effects, where the catalyst activity of the mixture surpasses that of the individual metals, have been reported for the material combinations of Cu/Fe [85–87], Ni/Fe [88], as well as Fe/Mo [89]. However, the combination of Pt/Ni significantly reduces the selectivity towards CO. Despite its higher activity compared to Pt/Co, the overall CO formation rate is lower [84]. In this case, the increased catalyst activity is related to the increase of the d-band center [84]. The higher the center of the

d-band relative to the fermi-level, the stronger the bond of the gas molecule (CO_2) at the surface of a transition metal [90]. In addition, doping Fe/Al_2O_3 with Co or Ni enhances catalyst activity and CO yield compared to the undoped Fe/Al_2O_3 catalyst. This improvement is attributed to better reducibility of the doped catalyst [91].

As before mentioned, metal carbides also exhibit catalytic activity for the RWGS reaction. However, their performance is highly dependent on catalyst doping: The activity of pure Mo_2C becomes significant only at temperatures above over 400 °C, where it achieves about 1/4 of the activity of the Cu/ZnO/Al_2O_3 catalyst. With the addition of 1 % Cu into the Mo_2C matrix, the catalyst becomes active at 300 °C with a higher catalytic activity compared to Cu/ZnO/Al_2O_3 catalyst [76]. This improvement is attributed to strong metal-support interactions, which enable electron transfer from Cu to the Mo_2C [14]. The high dispersion of Cu on Mo_2C also contributes to increased stability compared to Cu/ZnO/Al_2O_3 [76]. A similar effect can be observed with Co as doping material in Mo2C [92].

3.2.2 Alkali-Doped Catalysts

The addition of a small amount of alkali metals to the active metal phase enhances the dispersion of the active metal and improves CO_2 adsorption by increasing the electron density on the catalyst surface [93]. This effect is attributed to the interaction between the s-orbital of the alkali metal and the valence band of the active material. This interaction makes electrons from the alkali metal accessible to the active metal, thereby enhancing its basicity [93].

Among alkali metals, potassium (K) is the most commonly studied doping material in literature, followed by cesium (Cs) and sodium (Na). The addition of K into Pt leads to an increase in catalyst activity and selectivity compared to the Pt catalyst due to a weaker CO–Pt interaction and an increase of surface intermediate formate concentration [94]. A similar effect can be observed for Na doping of Pt catalysts [95]. Yang et al. [96] determined that a 16 wt % K loading in Pt achieves optimal CO_2 conversion and CO selectivity. In Cu-based systems, K significantly enhances CO_2 adsorption to an order of magnitude by providing new interfacial sites. This results in a larger formate coverage on the catalyst surface, which promotes CO formation compared to undoped Cu [97].

In a Co/CeO_2 system, K acts as a promoter by increasing CO_2 adsorption and facilitating Co reduction through an electron donation effect. This leads to enhanced conversion and selectivity [98]. K-doped Mo_2C catalysts show a significantly improved CO selectivity and stability due to enhanced CO_2 adsorption, reduced dissociation barrier, and a stabilizing effect for reduced Mo [75]. For WC as active catalyst, the addition of K also increases the CO selectivity for low temperatures although it reduces the CO_2 conversion compared to undoped WC [77]. The addition of Na has a more pronounced effect, further decreasing CO_2 conversion while achieving even higher CO selectivity [77].

In comparison, Cs has a larger ionic radius than K and Na, resulting in a higher electron accessibility due to its stronger basic nature [99]. For the Fe catalyst, the addition of Cs results in a higher CO_2 conversion at temperatures below 600 °C. For temperatures above 600 °C this effect diminishes [93]. The same effect was observed for Cs doping in a bimetallic Fe/Cu catalyst, yielding a higher conversion compared to a Cs-doped Fe catalyst [99].

3.2.3 Catalyst Support

The interaction between the active metal phase and the support material is a critical factor that can enhance the catalytic activity of supported catalysts. The role of the support material extends beyond providing structural stability, influencing the chemical and electronic properties of the active phase to varying extent [100]. Reducible oxides are particularly advantageous as support materials due to their ability to provide oxygen vacancies, which can actively participate in catalytic reactions [101, 102]. While thermodynamically all metal oxides can be reduced, the distinction between a reducible and non-reducible oxide is associated with the conditions required for oxygen vacancy formation [103]. Despite there is no strict definition defining the conditions for vacancy generation in reducible and non-reducible oxides [104, 105], Al_2O_3, SiO_2, CeO_2, TiO_2 and ZrO_2, Al_2O_3 and SiO_2 are considered non-reducible while CeO_2, TiO_2, and ZrO_2 are considered reducible [103, 106]. Although the non-reducible oxides Al_2O_3 and SiO_2 are often utilized as support material for RWGS reaction, they are primarily used as inert structural supports or as reference carriers in RWGS reaction studies [84, 85, 97, 102, 107].

Kim et al. [102] compared the performance of TiO_2 as reducible carrier material with Al_2O_3 as a non-reducible carrier for Pt-based catalysts. Their study demonstrated that TiO_2 acts as an active component when combined with Pt due to the formation of oxygen vacancies during H_2 reduction [102]. These vacancies serve as additional active sites at the metal-support interface, resulting in significantly higher CO_2 conversion compared to Pt/Al_2O_3 as catalysts [102]. Furthermore, thee authors concluded that the activity of the Pt/TiO_2 catalyst depends more strongly on the properties of the TiO_2 than on those of Pt itself [108]. Similarly, Sakurai et al. [109] investigated various carrier materials for Au-based catalysts in the RWGS reaction at 1 bar and 50 bar. Among the materials studied, Au/TiO_2 exhibited the highest catalytic activity, while Au/Al_2O_3, Au/Fe_2O_3, and Au/ZnO showed lower catalytic activities [109]. For Rh-based catalysts, TiO_2 was also found to be a superior support material [110]. Studies reported that the CO formation rate for Rh/TiO_2 was 10 to 100 times higher than that for Rh supported on MgO, Nb_2O_5, or ZrO_2 [110].

CeO_2, as another reducible oxide, exhibits catalytic activity for RWGS itself with high selectivity towards CO [111] but relatively low CO_2 conversion [112]. The formation of oxygen vacancies on the CeO_2 surface occurs more easily during reduction compared to other reducible oxides [113]. This, combined with the reversible Ce^{3+}/Ce^{4+} redox pair and basic surface properties, contributes to its favorable catalytic activity [114]. However, an additional metal is necessary to catalyze the reduction of the Ce, which would otherwise be re-oxidized by CO_2 [107]. For this reason, the distinction between CeO_2 as a doping material and as a support becomes blurred.

For Mn-Fe supported on Al_2O_3, the CO yield increases with Ce content up to 10 wt % [115]. Similarly, Pettigrew et al. [107] compared Pd/Al_2O_3 catalysts doped with different rare earth oxides, with highest conversion and selectivity observed for CeO_2. When CeO_2 serves as a support material for Co, CO_2 conversion increases significantly with rising Co content, while selectivity for CO decreases beyond a 2 wt % Co fraction due to the formation of large Co_3O_4 particles, which promote CH_4 formation [112]. For NiO supported on CeO_2, CO_2 conversion also improves with increasing NiO content, reaching optimal selectivity at 3 wt % [116]. Similarly, for In_2O_3 on CeO_2, the optimal composition for CO selectivity occurs at 44.6 mol. % CeO_2 [117]. Porosoff et al. [84] noted an increase in CO_2 conversion while the selectivity decreased to different extent for Pt-Co, Pt-Ni, and Pd-Ni catalyst supported on CeO_2 compared to those supported on Al_2O_3. Furthermore, they observed that CO selectivity varied correlating with the surface d-band center of the metal used [84].

Given the vast number of possible combinations of active metals, doping materials, and support structures, along with the inconsistency in reaction conditions across various studies, Tab. 2 provides an overview of peak CO_2 conversion, X_{CO2}, and CO selectivity, S_{CO}, for different catalytic systems reported in literature. To ensure clarity and focus, the table categorizes materials by temperature levels but does not explicitly subdivide data by pressure. This omission is justified by the fact that the RWGS reaction is largely insensitive to pressure. However, information on reaction pressure is still included alongside details of CO_2 conversion, selectivity, doping and support materials, and references for further context. Materials such as Li, K, Mo, Ce, Au, In, and La are not included in Tab. 2 as active catalytic materials due to their limited and isolated coverage in the available studies.

Despite the extensive number of publications exploring potential catalytic systems, only a limited selection of commercially available catalysts has been developed. For the state-of-the-art WGS reaction, traditionally employed catalytic materials include ferrochrome (Fe/Cr) for high-temperature shifts (up to 450 °C) and Cu/Zn/Cr for low-temperature shifts (up to 300 °C) [21, 130, 131]. These commercially available [132, 133] catalysts achieve a selectivity of 99 % towards CO_2 and H_2 production [131, 134], effectively suppressing CH_4 formation, which is thermodynamically favored. Both catalysts can also be utilized for the reverse reaction [101] provided that the respective temperature limitations are followed.

Two catalysts specifically designed for RWGS and available commercially by Clariant are the HyProGen® R-70 [135] and the ShiftMax® 100 RE [136]. Although Clariant has not disclosed details about the active material and composition, Lee et al. [137] described the HyProGen® R-70 as a "commercial Ni-based catalyst" for steam reforming. Similarly, INERATEC described the ShiftMax® 100 RE [136] as a nickel-based catalyst [138]. Other Ni-based catalysts initially developed for steam reforming have also been successfully deployed for the RWGS reaction. Examples include a Ni/Al_2O_3 catalyst [25] and a $Ni/Al_{12}O_{19}$ catalyst with traces of CaO, Na_2O, K_2O, and SiO_2 by Süd-Chemie Catalysts [139]. Since Clariant acquired Süd-Chemie in 2011, there is substantial evidence suggesting that the HyProGen® R-70 catalyst (10–20 % Ni on $Al_2O_3/CaO{\cdot}Al_2O_3$) is similar to the catalyst originally developed by Süd-Chemie. This hypothesis is supported by the fact that a reaction kinetic model developed for the Süd-Chemie catalysts [139] was used for designing the Sunfire reactor (covered in the next chapter), which employed Clariants HyProGen® R-70 catalyst (10–20 % Ni on $Al_2O_3/CaO{\cdot}Al_2O_3$) according to [33]. Another commercially available catalyst used for RWGS in the CAMERE®-Process is a 0.5 wt % Pt/Al_2O_3 catalyst from Thermo Fisher Scientific® (formerly Alfa Aesar®) [140].

One aspect that is not in the scope of this review are the costs of the respective catalytic material. For more information readers are referred to the available literature published by Juneau et al. [74].

3.3 Reaction Kinetic Models for RWGS

In Tab. 2, isolated values for CO_2 conversion and CO selectivity are provided for specific operational conditions. For reactor design, process modeling, simulation, and numerical optimization, a broader mathematical description for the reaction rate is essential. This description must account for a wide range of operational parameters [14]. For the RWGS reaction rate, three primary modeling approaches are commonly found in the literature: i) power law models provide a simple mathematical framework with limited physical interpretation, ii) Langmuir-Hinshelwood mechanisms that describe H_2-associated reaction pathways as surface reactions, involving adsorption, surface reaction, and desorption steps, with one step considered rate-determining, and iii) redox-mechanisms that depict the reaction as an interaction between gaseous species and oxygen vacancies on the catalyst surface [102]. Kim et al. compared all three approaches for Pt/Al_2O_3 and a $Pt\text{-}CeO/Al_2O_3$ catalyst [102]. They found that while power law and redox model predicted experimental data with high accuracy, the H_2 associative Langmuir-Hinshelwood model exhibited significant

Table 2. Overview of CO_2 conversion and CO selectivity for different catalytic metals and temperatures.

Material: Temperature:	Rh	Ni	Pt	Pd	Cu	Co	Ru	Fe
101–200 °C	Rh/SiO_2 $X_{CO2} = 52$ % $S_{CO} = 88.1$ % $H_2/CO_2 = 3$ 50 bar [118]	$Ni/LaZrO_2$ $X_{CO2} = 28$ % $S_{CO} = 98.5$ % $H_2/CO_2 = 1$ 1 bar [78]	$Pt/LaZrO_2$ $X_{CO2} = 40$ % $S_{CO} = 99.5$ % $H_2/CO_2 = 1$ 1 bar [78]	$Pd/LaZrO_2$ $X_{CO2} = 30$ % $S_{CO} = 99.2$ % $H_2/CO_2 = 1$ 1 bar [78]	$Cu/LaZrO_2$ $X_{CO2} = 28$ % $S_{CO} = 100$ % $H_2/CO_2 = 1$ 1 bar [78]			$Fe/LaZrO_2$ $X_{CO2} = 28$ % $S_{CO} = 100$ % $H_2/CO_2 = 1$ 1 bar [78]
201–300 °C	$Rh\text{-}Fe/TiO_2$ $X_{CO2} = 9.16$ % $S_{CO} = 28.4$ % $H_2/CO_2 = 1$ 20 bar [119]	$PdNi/CeO_2$ $X_{CO2} = 2.5$ % $S_{CO} = 60$ % $H_2/CO_2 = 2$ 1 bar [92]	$NaPt/ZrO_2$ $X_{CO2} = 29$ % $S_{CO} = 99$ % $H_2/CO_2 = 4$ 20 bar [95]	$PdNi/CeO_2$ $X_{CO2} = 2.5$ % $S_{CO} = 37.5$ % $H_2/CO_2 = 2$ 1 bar [92]	Cu/CeO_2 $X_{CO2} = 18$ % $S_{CO} = 100$ % $H_2/CO_2 = 1$ 1 bar [120]	Co/Mo_2C $X_{CO2} = 9.5$ % $S_{CO} = 98.1$ % $H_2/CO_2 = 1$ 1 bar [92]		
301–400 °C		RuNi/CeZr $X_{CO2} = 53$ % $S_{CO} = 93$ % $H_2/CO_2 = 4$ N.A. bar [121]		$Pd/LaZrO_2$ $X_{CO2} = 20$ % $S_{CO} = 100$ % $H_2/CO_2 = 3$ 1 bar [69]	Cu/CeO_2 $X_{CO2} = 52$ % $S_{CO} = 95$ % $H_2/CO_2 = 9$ 1 bar [80]	KCo/CeO_2 $X_{CO2} = 13$ % $S_{CO} = 100$ % $H_2/CO_2 = 1$ 1 bar [98]	RuNi/CeZ $X_{CO2} = 53$ % $S_{CO} = 93$ % $H_2/CO_2 = 4$ N.A. bar [121]	$FeMo/Al_2O_3$ $X_{CO2} = 45$ % $S_{CO} = 85$ % $H_2/CO_2 = 4$ 1 bar [93]
401–500 °C		Ni/CeO_2 $X_{CO2} = 28$ % $S_{CO} = 80$ % $H_2/CO_2 = 1$ 1 bar [122]	Pt/TiO_2 $X_{CO2} = 39$ % $S_{CO} = 100$ % $H_2/CO_2 = 3/2.1$ N.A. bar [14]	$Pd/LaZrO_2$ $X_{CO2} = 33$ % $S_{CO} = 100$ % $H_2/CO_2 = 3$ 1 bar [69]	Cu/CeO_2 $X_{CO2} = 50$ % $S_{CO} = 100$ % $H_2/CO_2 = 4$ 1 bar [123]	KCo/CeO_2 $X_{CO2} = 32$ % $S_{CO} = 100$ % $H_2/CO_2 = 1$ 1 bar [98]	Ru/CeO_2 $X_{CO2} = 28$ % $S_{CO} = 100$ % $H_2/CO_2 = 1$ 1 bar [124]	$CsFe/Al_2O_3$ $X_{CO2} = 50$ % $S_{CO} = 93$ % $H_2/CO_2 = 4$ 1 bar [93]
501–600 °C		Ni/Al_2O_3 $X_{CO2} = 50$ % $S_{CO} = 75$ % $H_2/CO_2 = 2$ 30 bar [125]	Pt/TiO_2 $X_{CO2} = 22$ % $S_{CO} = 100$ % $H_2/CO_2 = 4$ N.A. bar [126]		Cu/CeO_2 $X_{CO2} = 70$ % $S_{CO} = 100$ % $H_2/CO_2 = 4$ 1 bar [127]	KCo/CeO_2 $X_{CO2} = 37$ % $S_{CO} = 100$ % $H_2/CO_2 = 1$ 1 bar [98]		$CsFe/Al_2O_3$ $X_{CO2} = 60$ % $S_{CO} = 98$ % $H_2/CO_2 = 4$ 1 bar [93]
601–700 °C		$Ni/Ce_{0.75}Zr_{0.25}O_2$ $X_{CO2} = 62.5$ % $S_{CO} = 99.5$ % $H_2/CO_2 = 3$ 1 bar [128]	Pt/TiO_2 $X_{CO2} = 40$ % $S_{CO} = 96$ % $H_2/CO_2 = 4$ N.A. bar [126]					$CsFe/Al_2O_3$ $X_{CO2} = 72$ % $S_{CO} = 100$ % $H_2/CO_2 = 4$ 1 bar [93]
701–800 °C		$Ni/CeO_2\text{-}Al_2O_3$ $X_{CO2} = 59$ % $S_{CO} = 94$ % $H_2/CO_2 = 3$ 13.79 bar [115]	Pt/TiO_2 $X_{CO2} = 50$ % $S_{CO} = 94$ % $H_2/CO_2 = 4$ N.A. bar [126]					$CsFe/Al_2O_3$ $X_{CO2} = 75$ % $S_{CO} = 100$ % $H_2/CO_2 = 4$ 1 bar [93]
>800 °C		NiO/silica $X_{CO2} = 55$ % $S_{CO} = 100$ % $H_2/CO_2 = 1$ 1 bar [129]	Pt/TiO_2 $X_{CO2} = 38$ % $S_{CO} = 85$ % $H_2/CO_2 = 4$ N.A. bar [126]					

deviations from the experimental results [102]. Similar findings were reported by Jadhav et al. [140] for a commercial Pt/Al_2O_3 catalyst later employed in the CAMERE® process, where a redox model aligned well with experimental data, while a H_2-assisted kinetic model yielded implausible parameters.

For Cu-based catalysts direct dissociation is often reported to be the primary reaction pathway for the RWGS reaction [141]. However, the reaction order changes depending on the operating conditions [24]. Ernst et al. [142] reported for a pure Cu surface that at high H_2 partial pressures (p_{H2}:$p_{CO2} > 10$), the reaction is independent of H_2

Table 3. Overview of different modeling approaches of the RWGS reaction and available models in literature.

Reaction kinetic model	Modeling approach	Mechanism	Published for catalyst:
Power law	Mathematical description	–	Pt/Al_2O_3, $Pt\text{-}CeO/Al_2O_3$ [102] Cu [142] Ni/Al_2O_3, Co/Al_2O_3, Fe/Al_2O_3, MoS_2, WS_2 [145] Pd/Al_2O_3, $Pd\text{-}CeO_2/Al_2O_3$ [107] Ni/Al_2O_3 [25], $Ni/Al_{12}O_{19}$ [139]
Langmuir-Hinshelwood	Subsequent adsorption, surface reactions, desorption Identification of rate-determining step	H_2-mediated	Pt/Al_2O_3, $Pt\text{-}CeO/Al_2O_3$ [102] Cu/SiO_2 [144]
Redox mechanism	Pseudo reaction with surface oxygen vacancy	Direct dissociation	Pt/Al_2O_3, $Pt\text{-}CeO/Al_2O_3$ [102, 140] $Cu/Zn/Al_2O_3$ [143] $FeMo/Al_2O_3$ [146]

the partial pressure. For medium-high H_2 partial pressures ($10 > p_{H2}:p_{CO2} > 2$), the reaction rate is nearly independent of CO_2 partial pressure but close to first order for H_2 partial pressure when modeled using the power law function [142]. At low H_2 partial pressures ($0.75 > p_{H2}:p_{CO2}$), the rate of reaction exceeds first order with respect to H_2, indicating that the activity of the Cu phase for CO_2 dissociation strongly depends on the H_2 coverage [142]. Consequently, a pure redox reaction model is inadequate for RWGS reaction on Cu. Similar trends were observed for Cu in combination with ZnO on Al_2O_3 support by Ginés et al. [143] for various H_2-to-CO_2 ratios. For Cu nanoparticles on SiO_2, Chen et al. proposed a formate-based (H_2-assisted) reaction mechanism using a Langmuir-Hinshelwood-type reaction kinetic model [144].

Osaki et al. [145] studied Ni/Al_2O_3, Co/Al_2O_3, Fe/Al_2O_3, MoS_2, and WS_2, reporting activation energies and reaction orders for power law models. They found that high H_2 reaction orders correlated with high CH_4 selectivity for Ni/Al_2O_3 and Co/Al_2O_3, while low H_2 reaction orders correlated with high CO selectivity for Fe/Al_2O_3, MoS_2, and WS_2 [145]. Pettigrew et al. [107] observed similar correlations for Pd/Al_2O_3 and $Pd\text{-}CeO_2/Al_2O_3$ catalysts in their power law models. For $FeMo/Al_2O_3$ catalysts, Ghodoosi [146] et al. developed a redox reaction kinetic model. Wolf et al. [25] published intrinsic power law reaction kinetics for RWGS for a commercial Ni/Al_2O_3 catalyst and compared experimental results of 3-mm catalyst particles with a simulation including intrinsic power law kinetic and inner and outer mass transfer with good agreement.

The same research group developed a kinetic model for the commercially available $Ni/Al_{12}O_{19}$ with traces of CaO, Na_2O, K_2O, and SiO_2 by Süd-Chemie Catalysts [139]. This kinetic model was later utilized in designing the RWGS reactor in the Sunfire project, discussed in the next chapter. The following Tab. 3 presents an overview of the previously discussed reaction kinetic models for the RWGS reaction.

3.4 Catalyst Stability

The activity of a catalyst decreases over time as a result of different processes. For RWGS catalyst, the most significant deactivation mechanisms are metal sintering, coke deposition, and sulfur poisoning [14]. While metal sintering and coke formation depend on the active metal itself, metal-support-interaction and structural properties such as active surface area and porosity [139], sulfur poisoning is solely related to the purity of the reacting gas [14] and will therefore not be covered in detail.

Metal sintering describes the reduction of active surface area due to a minimization of free surface energy at elevated temperatures [40]. This leads to a decrease in dispersion of the active metal, thereby reducing catalyst activity and CO selectivity [76, 82, 93]. Coke deposition also reduces the active surface of the catalyst by blocking active centers. It is caused by the Boudouard reaction and methane pyrolysis at elevated temperatures, as described earlier. Theoretically, coke deposition can be removed by altering the reaction condition to induce methanation, gasification, reverse Bourdouard reaction [14], or combustion with oxygen [30]. Metal sintering can be mitigated by using a layered structure of the active metal, e.g., in perowskite-type crystal structures [14], or by employing hydrotalcite structures that provide higher metal dispersion and improved resistance to coke deposition [147]. Embedding the active metal in zeolites has also been shown to prevent sintering, as demonstarted for Pt [96] and Ni [129]. Since sintering effects correlate with the melting temperature of the active metal [15], adding a metal with a higher melting point than the original active metal is an effective strategy to prevent both sintering and coke formation [89]. For example, the addition of Mo in Fe catalyst enhances metal dispersion while inhibiting sintering [89], and Fe addition suppresses sintering in Cu [85, 86].

Coke formation is generally more pronounced on Fe, Cu, and Ni surfaces than on the surfaces of noble metals like Pt, Ru, or Rh at temperatures above 500 °C [142]. Basic doping

materials such as La or Mg have been shown to reduce coke formation effectively [14]. Since gasification of coke deposition involves a redox mechanism sensitive to the availability of surface oxygen [148], the use of reducible oxides can not only increase catalyst activity due to a higher number of oxygen vacancies but also reduce coke formation by accelerating the gasification reaction [14].

It is important to emphasize that stability tests for catalysts under RWGS conditions are typically conducted over 40–100 h [76, 86, 92, 93, 125, 126, 139, 149]. No long-term stability data is available at this time, and even a small rate of coke formation can cause a large decrease in catalyst activity over time. For low-temperature RWGS (<400 °C), many catalysts in literature show little to no decrease in activity [75, 139]. Zhuang et al. [149] observed a decline in CO_2 conversion by one-third over 70 h at 450 °C for Cu-based catalysts, while at 700 °C the reactor became clogged with carbon deposition after only 25 h [149]. Although Ru doping reduced coke formation, the reactor was clogged after 50 h. For the Cu catalyst, Zhang et al. [76] reported only 25 % of the initial CO_2 conversion after 15 h at 600 °C using ZnO/Al_2O_3 as support material. By switching to MoC as support material, the catalyst stability improved, with 75 % of the initial conversion after 40 h [76]. For $FeCu/Al_2O_3$, two-thirds of the initial CO_2 conversion remained after 100 h operation at 600 °C [86].

A CS-doped Fe/Al_2O_3 catalyst retained its initial activity over 40 h at 550 °C [93] as well as a Pt/TiO_2 catalyst over 80 h at 600 °C [126]. A $Ni/Al_{12}O_{19}$ catalyst showed constant activity over 100 h at 450 °C, but at 650 °C the activity decreased by one-third within 6 h with a reported coke yield from CO_2 of 0.0027 % [139]. Vasquez et al. [125] compared Ni/Al_2O_3 catalysts with Rh-based catalysts. For Ni catalysts at 505 °C and 30 bar, an initial stabilization period was observed in which the activity decreased by 50 % over 40 h, while CO selectivity increased [125]. After stabilization, the activity remained constant for 80 h [125]. Ting et al. [150] conducted activity measurements over 1000 h for Re/TiO_2, $Cu/ZnO/Al_2O_3$, and $Fe/Cr/CuO_x$ catalysts at 500 °C. The CO_2 conversion of $Fe/Cr/CuO_x$ catalysts decreased to 25 % of the initial activity in less than 200 h, while the activity of $Cu/ZnO/Al_2O_3$ dropped to one-third of the initial value [150]. In contrast, the activity of Re/TiO_2 remained almost constant over more than 1000 h of operation [150].

Catalyst screening for the CAMERE process, which will be discussed in the following chapter, demonstrated that the well-known high-temperature WGS catalyst Fe_2O_3/Cr_2O_3 performs poorly under RWGS conditions [151]. In lab-scale experiments, CO_2 conversion decreased by over 10 % in 75 h due to a reduction of Fe_2O_3 and Cr_2O_3 to Fe_3O_4 and $FeCr_2O_4$ [151]. Furthermore, metal carbide (F_3C) formation was observed [151]. Continued experiments in a tubular reactor resulted in clogging caused by coke formed during the reaction, leading to a pressure increase and a subsequent rise in CH_4 selectivity to 98 % [151].

4 RWGS Projects and Practical Application

Lab-scale experiments with different catalysts in small scale provides limited indication of the potential success of full-scale facilities, particularly regarding long-term catalyst stability, efficiency, and operability. This is primarily due to more pronounced coke formation and metal dusting in larger systems compared to lab-scale experiments, as well as additional challenges such as heating methods, reactor design, and material stability. Therefore, this chapter provides an overview of projects and sites that have progressed beyond lab scale to pilot scale.

4.1 CAMERE

The CAMERE process refers to a specific method for carbon dioxide hydrogenation to produce methanol via an RWGS reaction (carbon dioxide hydrogenation to form methanol via a reverse water-gas shift reaction) but is also associated with a pilot plant constructed in South Korea by the Pohang Iron and Steel Company (POSCO) and the Korea Electric Power Research Institute (KEPRI), as reported in 2013 [152, 153]. The plant consisted of an RWGS reactor, a water separation unit, a pressure amplifier, and a methanol reactor with product separation and gas recycle as illustrated in Fig. 5. The target production capacity was 100 kg/day of methanol. The CAMERE process was combined with a pilot plant for CO_2 separation from a power plant [152].

The RWGS reactor consisted of an electrically heated single reactor tube (5 cm inner diameter, 120 cm length) filled with a $ZnAl_2O_4$ catalyst (Zn:Al = 2:1), which had been identified as sufficiently stable and active for CO_2 conversion in prior lab-scale studies [151, 154]. The RWGS reactor operated at atmospheric pressure and temperatures between 600 °C and 700 °C with a feed molar ratio of CO_2:H_2 = 1:3 and a feed rate of 150 $L_{gas}g_{cat}{}^{-1}h^{-1}$ [152]. At temperatures above 600 °C, CO_2 conversion to CO exceeded 60 % with the catalyst activity rarely decreasing over nine days of operation [152].

To assess the RWGS reactor's impact on methanol production, the pilot plant was operated both with and without using the RWGS reactor. In the configuration without the RWGS reactor, the CO_2/H_2 mixture was compressed and fed directly into the methanol unit. The results showed that integrating the RWGS reactor more than doubled the methanol yield (70 % vs. 32 %) compared to direct CO_2-based methanol synthesis (RWGS reactor bypassed). This improvement was attributed to a significantly lower gas recycle and thereby reduced purge stream [152]. At peak performance, 75 kg methanol per day were produced out of 100 kg CO_2 [152]. Based on the experimental results, cost calculations were performed for various production scales, indicating that methanol could be produced at a cost of approximately $300 per ton using the CAMERE process in 2013 [152].

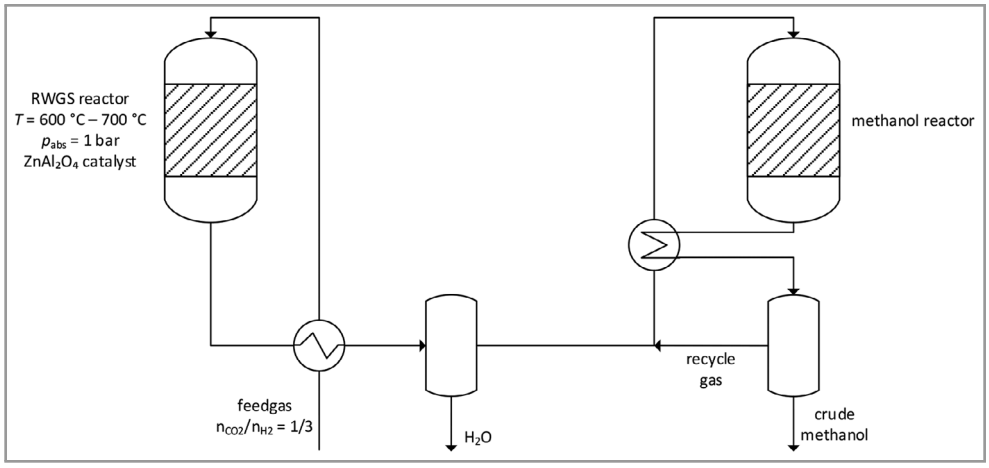

Figure 5. Simplified flowsheet of the CAMERE process based on [152].

4.2 INERATEC Power-to-Liquid(PtL) Process

The company INERATEC GmbH operates a power-to-liquid plant housed in a cargo container at the Karlsruhe Institute of Technology (KIT) in Germany. The plant features an electrically heated RWGS reactor, followed by a Fischer-Tropsch reactor, designed to produce up to 200 L of synthetic fuel per day [155]. Detailed information regarding the reactor design and its operational performance is not available.

For the ReFuels research project (2019–2022), about 70 L of Fischer-Tropsch product were produced by INERATEC. However, according to the final report, the RWGS reactor was not in operation during the test run and CO from gas cylinders was used for the Fischer-Tropsch synthesis [156, 157]. In addition, a technical concept was developed to evaluate production costs and to assess the economic feasibility of integrating a power-to-fuel process into the MiRO refinery [156]. The target was to produce 50 000 t of liquid product per year from CO_2 and H_2 [156]. The RWGS process was considered only at a low level of detail due to its low technology readiness level (TRL < 6), with syngas production via methanation and dry reforming being preferred [156].

In 2022, INERATEC and Clariant announced a strategic partnership to offer a container unit for RWGS reaction with Clariants ShiftMax® 100 RE catalyst (see previous section) [138]. The next step involves constructing a pilot-scale power-to-liquid plant at the Industriepark Höchst in Frankfurt, Germany. This facility is expected to produce 2500 t of e-fuels per year [158].

4.3 CO_2rrect

The CO_2rrect project, conducted between 2010 and 2013 and funded by the German Federal Ministry of Education and Research (BMBF), aimed to develop and construct an RWGS reactor at a technical pilot-plant scale. While this reactor was not realized, two lab-scale reactors featuring different heating concepts were developed and tested for RWGS: direct electrical heating via resistance heating of catalyst-coated structures and microwave heating combined with partial H_2 combustion using oxygen [159].

For the electrical resistance heating concept, Bayer Technology Services GmbH (BTS) designed a pilot-plant setup consisting of 22 catalyst-coated heating coils made of Kanthal and 11 catalyst-coated honeycomb structures made of Al_2O_3. The reactor was designed to be operated at a temperature between 800 °C and 1000 °C and a pressure of 10 bar. In lab-scale experiments, a single coated heating coil was used. For a feed gas flow rate of 4 m^3h^{-1} with an H_2/CO_2 molar ratio of 1.5, CO_2 conversions of 20–30 % were achieved at 6 bar, demonstrating the functionality of this heating concept for the RWGS reaction. However, a broad temperature distribution across the heating coil, ranging between 880 °C and 1067 °C was detected. Additionally, a solid brown coating consisting of catalyst metals indicated the occurrence of metal dusting [159].

For the microwave heating concept combined with hydrogen combustion, the University of Stuttgart developed a reverse-flow tube bundle reactor consisting of seven reaction tubes (Al_2O_3) inside a fused silica housing. The upper 200 mm of each tube was coated with catalyst on both the inside and outside, while the lower part was left uncoated to allow for countercurrent heat recovery. Above the reactor tubes, an induction core for microwave heating was installed and oxygen was supplied to the reaction zone via six smaller tubes at the start of the catalyst coating, with additional oxygen provided at the top of each reaction tube [159].

In the countercurrent reactor setup, a feed gas flow of 1 L min^{-1} entered each tube's uncoated section at the inside, flowing upwards towards the catalyst-coated part of the reactor tube while being heated by product gas flowing downwards outside of the reactor tube. At the catalyst side, microwave heating or hydrogen combustion maintained the reaction temperature at approximately 1000 °C. With hydrogen combustion, a CO_2 conversion of 38 % was observed. Equilibrium analysis revealed that the CO_2 conversion correlated with the average catalyst bed temperature rather

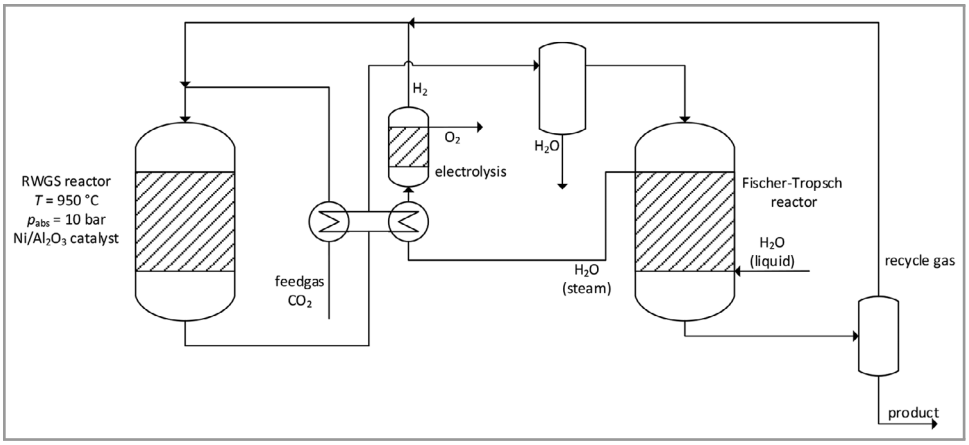

Figure 6. Simplified flowsheet of the Sunfire PtL process based on [33].

than the flame temperature, providing valuable insights for similar heating concepts. However, long-term operability was not evaluated [159].

Microwave heating, combined with partial H_2 combustion, was not tested in the same setup due to insufficient heat transfer when an induction core was installed. For the microwave heating concept, a fixed-bed reactor was utilized. Due to inhomogeneities in the packing material as well as a self-accelerated heating with microwaves, a broad temperature distribution across the axial direction and an unpredictable hot-spot formation was observed. Despite achieving a high CO_2 conversion of 49 % under stoichiometric conditions, the authors concluded that this thermal behavior of the reactor was "not tolerable" for technical application as it would require a local measurement and control of temperature that would rarely be feasible [159].

4.4 Sunfire

Sunfire, a company established in 2010, developed a process integrating an RWGS reactor with Fischer-Tropsch synthesis to enable efficient heat recovery. Starting with a 28 g h^{-1} laboratory-scale setup, the process was scaled up to an 8.5 kg h^{-1} naphtha and diesel production plant, operated during a research project between 2012 and 2017. During the project, Sunfire designed and operated an RWGS reactor with a synthesis gas output capacity of 224 kW (51 kg h^{-1}). The process encompassed CO_2 and H_2O supply, reaction units, and product separation with off-gas recycling. [33]

To preheat the CO_2 feedstock, hot synthesis gas from the RWGS reactor was utilized, while H_2O was evaporated as a coolant in the Fischer-Tropsch reactor and subsequently overheated, as illustrated in Fig. 6. After electrolysis, CO_2 and H_2 were electrically preheated inside the RWGS reactor. The reactor itself featured five electric heating stages (six electrical heaters with 5.5 kW each) each followed by a catalyst bed to ensure a sufficient reactant temperature during the endothermic RWGS reaction at 950 °C. After RWGS, water was separated from the synthesis gas before entering the Fischer-Tropsch reactor. The product stream of the Fischer-Tropsch reactor was separated into liquid and gaseous products with the latter one being repressurized and fed back into the RWGS reactor as recycle [30, 33].

Initially, the RWGS reactor was designed for operation at 30 bar to enable Fischer-Tropsch synthesis at 25 bar without the need for a synthesis gas pressure amplifier. As catalyst, the formally mentioned Clariants HyProGen® R-70 catalyst (3.2 mm × 3.2 mm; 10–20 % Ni on Al_2O_3/CaO·Al_2O_3) was used. Preliminary testing was conducted in laboratory scale with a commercially available Ni/$Al_{12}O_{19}$ catalyst by Süd-Chemie Catalysts to develop a reaction kinetic model and investigate catalyst deactivation. To reduce material stress under high-temperature conditions, the RWGS reactor setup was placed in an isolated pressure dome flushed with nitrogen [30, 33].

In the first part of the project, it became evident that the reactor setup faced issues due to insufficient isolation at high pressures. Consequently, the maximum pressure of the RWGS reactor was reduced to 10 bar. After reaching steady-state operation, a rapid pressure increase was observed (8.5 to 22 bar) due to coke formation, which led to metal dusting and clogging of the heat exchangers. Attempts to remove the deposits through steaming or combustion with oxygen were unsuccessful, and the RWGS reactor had to be shut down after 240 h of operation due to increasing pressure and failure of multiple electrical heaters. During this phase, a maximum thermal efficiency of 26.5 % was achieved with a CO_2 conversion of 60 % [30, 33].

Analysis of the deposits revealed the presence of metal carbides caused by coke reacting with the interior reactor surfaces, leading to material degradation. Reactor material (Fe, Cr) and material from reactor isolation and carrier structure have also been found as deposition on the catalyst. It was concluded that carbon deposition is inevitable and measures are required to mitigate metal dusting and clogging. Consequently, reactor design and material, isolation, synthesis gas cooler, and electrical heaters were redesigned. The operating pressure was maintained at 10 bar to limit coke formation, and a synthesis gas compressor was added

between the RWGS and Fischer-Tropsch reactors to compensate for the reduced pressure. Additionally, a burn-off/purge concept was implemented for the heat exchangers. With this revised setup, operation at full load and continuous operation over 1600 h was demonstrated. Although burn-off of the deposits was again unsuccessful using CO_2 or O_2, increased gas flow at elevated temperatures purged the deposits, restoring heat flux within the heat exchangers. This purging procedure was performed regularly to maintain continuous operation. The inside of the heat exchanger interior was not analyzed for metal carbides afterwards, but coke deposits were detected in the cooling system. Since coke burn-off was not successful, it seems likely that those depositions contained metals as in the first part of the project [30, 33].

During operation, CO_2 conversion in the RWGS reactor reached 64 % in linear mode and 58 % in recycle mode, while the overall CO_2 conversion of the integrated process was 47 % in linear mode and 75 % in recycle mode. The maximum thermal efficiency achieved was 64 % in linear mode and 67 % in recycle mode. The RWGS reactor also demonstrated load flexibility, producing 16.3 kg h^{-1} of synthesis gas at low load in linear mode and 59.5 kg h^{-1} at high load in recycle mode. Sunfire concluded that the RWGS process achieved a TRL of 6, corresponding to prototype demonstration in a relevant operational environment [30, 33].

5 Potential Future of RWGS in Chemical Industry

As already mentioned in the previous chapter, INERATEC is building an pilot-scale PtL plant in Frankfurt, Germany (Industriepark Höchst), with the goal of producing 2500 t of e-fuels per year [158]. Another company with the aim of commercializing power-to-fuel application with RWGS is Norsk e-fuel.

Norsk e-fuel was founded in 2019 with the goal of establishing industrial production of sustainable aviation fuels. The founding partners are Sunfire, Climeworks, Paul Wurth, and Valinor [160]. To achieve this goal, the company has secured three production sites: Project Mosjøen in Nesbruket, Vefsn Municipality, Norway for a production of 50 000 m^3 renewable fuel, project Rauma in the port of Rauma, Finland for 100 000 m^3 of e-fuel, and Nyland Øst, Vefsn Municipality in Norway [161]. Norsk e-fuel is following a dual approach with two parallel production lines in its first plant: One "innovative state-of-the-art approach" featuring electrolysis and the RWGS reaction before Fischer-Tropsch synthesis, and a "cutting-edge approach" incorporating Co-SOC electrolysis ahead of Fischer-Tropsch synthesis [162]. Initially, the production target was set at 12 500 m^3 per year, with the RWGS line scheduled to start operation in 2024 [163]. Paul Wurth S.A. of the SMS Group has been announced as a partner for the engineering and design of the e-fuel production facilities and for developing the electrically heated RWGS unit together with Axens [164, 165].

Besides the reported projects for the production of renewable fuels, the RWGS reaction can serve as a supplement for synthesis gas production in the chemical industry. By integrating RWGS in different state-of-the-art or innovative processes, efficiency can be improved, and synergetic advantages can be realized. Two concepts illustrating this potential are presented in the following.

BASF SE filed a patent for the parallel preparation of hydrogen, carbon monoxide, and a carbon-comprising product using methane and CO_2 as feedstock [166]. A simplified flowchart of the process is displayed in Fig. 7. In this concept, BASF's methane pyrolysis process [167] generates the feed material for an RWGS reactor. Within the pyrolysis reactor, methane is converted into solid carbon and H_2. The produced hydrogen and unreacted CH_4 from the pyrolysis reactor are fed into an adiabatic

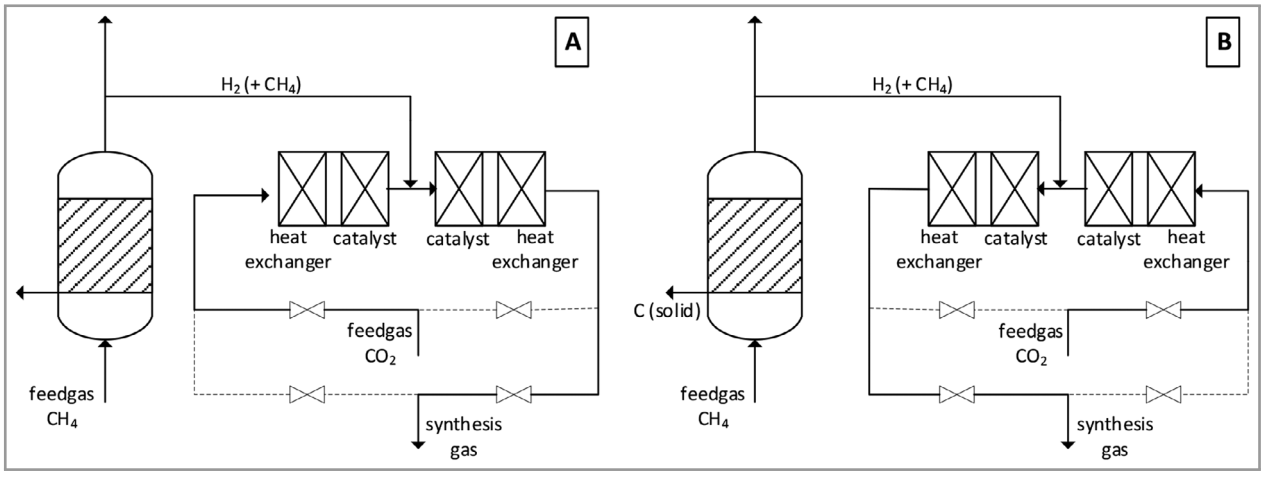

Figure 7. Simplified flowsheet for the parallel preparation of hydrogen, carbon monoxide, and a carbon-comprising product using methane and CO_2 as feedstock based on [166].

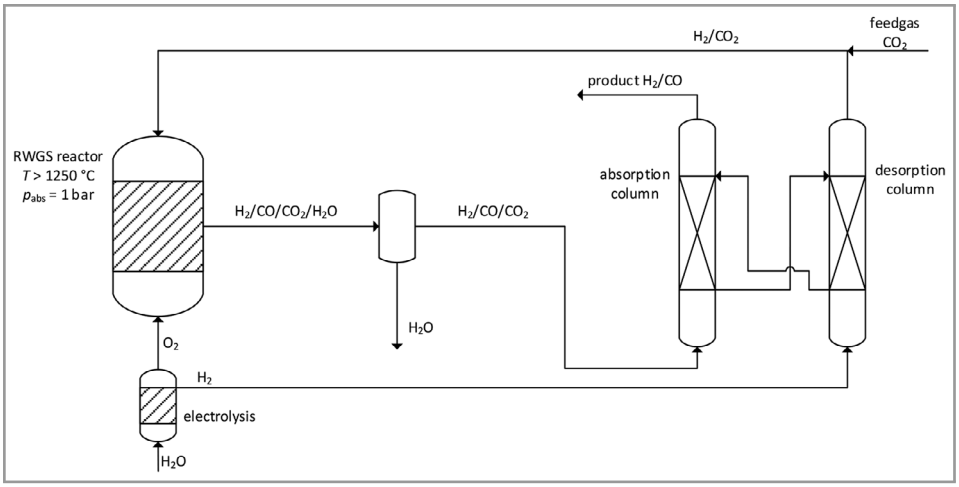

Figure 8. Simplified flowsheet for the Linde integrated RWGS process based on [35].

RWGS fixed-bed reactor, where they are mixed with preheated CO_2 as indicated in Fig. 7 (A). RWGS reaction takes place at temperatures between 800 °C and 1000 °C using a honeycomb-immobilized catalyst or a spherical-shaped catalyst. To optimize energy efficiency, the product gas exiting the RWGS reactor heats an inert packing material located downstream of the catalyst zone. After 1–5 min, the flow direction is reversed so that the preheated inert packing material heats the incoming CO_2 (Fig. 7B). The CO_2 flows through the previously used catalyst bed and is again mixed with H_2/CH_4 from the pyrolysis reactor. The mixture is then fed into a catalyst bed on the opposite side, repeating the process while preheating the inert packing material on the opposite end [166].

Linde integrated a thermal RWGS reactor into a CO_2-scrubbing process in a patent filed in 2021 [35], illustrated in Fig. 8. In a first step, electrolysis generates H_2 and O_2. H_2 is used as stripping gas in the desorption column of the CO_2 scrubbing process, while O_2 is fed into the RWGS reactor. The H_2 and CO_2 mixture from the desorption column is fed into the RWGS reactor as well, where partial combustion of the hydrogen provides reaction enthalpy for thermal RWGS reaction at temperatures above 1250 °C. At these temperatures, coke and methane formation are thermodynamically suppressed. The resulting product mixture is cooled and water is condensed. The remaining gas, consisting of CO_2, CO, and H_2, is fed into the absorption column of the CO_2 separation unit, where CO_2 is removed, so that the final product of this concept is a CO/H_2 mixture [35].

6 Summary

In summary, this literature review highlights the potential of the RWGS reaction as key process for renewable synthesis gas production, serving as a link for integrating renewable carbon sources into existing chemical and fuel production processes. Thermodynamically, high temperatures are essential for overcoming thermodynamic barriers and suppressing unwanted side reactions, including methane and coke formation, particularly under elevated pressures. To reduce the reaction temperatures that are necessary for thermal CO_2 conversion, and thereby lowering the energy input for RWGS, catalytic RWGS presents a viable solution.

This review explores RWGS reaction mechanisms involving various surface intermediates and links them to the catalytic performance of active materials. It is demonstrated that catalytic performance correlates with the oxygen affinity of the catalyst material, and that highly selective catalysts must be deployed at short contact times to avoid the formation of byproducts.

Different reaction kinetic models, including power law, Langmuir-Hinshelwood, and redox mechanisms are evaluated for their ability to predict RWGS behavior under different conditions for various catalysts. Although lab-scale investigation showed promising results, metal dusting as a result of coke formation has been identified as a significant challenge in technical application across multiple research projects. Considering the reaction conditions derived in this literature review, the RWGS reaction shows significant similarity to steam reforming, with increased complexity due to the absence of steam. For efficient CO production via RWGS, achieving high CO_2 conversion and minimizing CH_4 concentration are crucial, which aligns with the objectives of steam reforming, where high CH_4 conversion and low CO_2 concentration are desired.

Also similar to RWGS, coke formation remains a significant challenge in steam reforming [19, 168, 169]. Since coke formation can not be eliminated completely, optimized materials and coke removal strategies are necessary and have been demonstrated to work effectively for a limited time in pilot-scale application. Consequently, the RWGS process is estimated to have achieved a TRL of 6, supported by similar evaluation (TRL 6) that has been published by Jänisch et al. [170].

To raise the RWGS process beyond its current TRL of 6, a targeted strategy has to focus on long-term catalyst stability, reactor integration, and process design. A crucial lever for advancing TRL is the selection and further optimization of catalytic systems that maintain high CO selectivity and CO_2 conversion while minimizing deactivation and coke formation over technically relevant operational periods. Ni-based catalysts appear to be promising options due to their proven performance at high temperatures (especially in SMR), commercial availability, and cost-effectiveness. This assessment also seems logical given the partnership between INERATEC and Clariant as described earlier.

Other catalysts discussed in literature, such as supported catalysts on reducible oxides (e.g., CeO_2, TiO_2) or bimetallic and carbide-based systems, have shown competitive selectivity and resilience against coking at moderate temperatures; however, extended catalyst testing information in larger scale is missing. Additionally, SMR offers a valuable blueprint for reactor material selection, heat integration strategies, and catalyst regeneration in terms of coke mitigation techniques, which may be applicable to RWGS scale-up. For the reaction conditions of the RWGS, analogously to the SMR the addition of steam and subsequent condensation can be a promising strategy for the suppression of coke formation, although it limits the achievable equilibrium conversion and increases the energy demand as well as investment and operating costs.

As an outcome of the Sunfire project, the reaction pressure in the RWGS reactor should be limited to avoid material failure and by-product formation [30, 33]. To surpass TRL 6, RWGS technologies have to be transferred from lab- and pilot-scale demonstration to stable, continuous pilot operation under industrially relevant conditions. This transition to TRL 7 might just be in progress with "INERATEC's first commercial-scale plant, the largest PtL plant of its kind in Europe and worldwide" in Frankfurt, Germany, that started production in May 2025 [171].

Acknowledgment

Open access funding enabled and organized by Projekt DEAL.

Rafael Becka has been working as a research associate at the Sub-Institute for Chemical Energy Carriers – Fuel Technology of the Engler-Bunte Institute (EBI ceb) at the Karlsruhe Institute of Technology (KIT) since 2019, following his master's degree in Process Engineering at the Rheinisch-Westfälische Technische Hochschule Aachen (RWTH Aachen) and his master's thesis at the Jülich Research Center (FZJ). His work at EBI ceb focuses on the catalytic-chemical synthesis of CO_2-based energy carriers, with a particular emphasis on methanol synthesis.

Siegfried Bajohr studied chemical engineering at the University of Karlsruhe and has been responsible for the field of catalytic-chemical processes in fuel conversion at the Chemical Energy Carriers and Fuel Technology branch of the Engler-Bunte-Institut at KIT since his doctorate in 2002. In his function as senior lecturer, his research and teaching activities focus on the field of catalytic processes and on the generation, conversion, and utilization of chemical energy sources with novel reactor concepts.

Thomas Kolb held the Chair for Process Engineering of Chemical Energy Carriers at the Faculty of Chemical and Process Engineering at the Karlsruhe Institute of Technology (KIT). He headed the Sub-Institute for Chemical Energy Carriers – Fuel Technology of the Engler-Bunte Institute (EBI ceb) at KIT as well as the Gasification Technology Department of the Institute for Technical Chemistry (ITC vgt) at KIT. Prof. Kolb was the head of the Gas Technology Division of the Research Center of the German Association for Gas and Water (DVGW-EBI-gt) at the Engler-Bunte Institute. As of October 1, 2024, Prof. Kolb retired but continues to be scientifically active at both EBI ceb and ITC vgt.

Symbols used

$\Delta_R G$	[kJ mol^{-1}]	reaction Gibbs free energy
$\Delta_R H^0$	[kJ mol^{-1}]	standard enthalpy of reaction
G	[kJ mol^{-1}]	Gibbs free energy
K_{eq}	[–]	chemical equilibrium constant
$\{N_i\}$	[mol]	composition
n_i	[mol]	amount of component i

$n_{i,0}$	[mol]	amount of component *i* at the beginning
p	[Pa]	pressure
p_i	[mol]	partial pressure of component *i*
R	[J mol^{-1}K^{-1}]	molar gas constant
S	[kJ mol^{-1}K^{-1}]	entropy
S_i	[–]	selectivity towards component *i*
T	[K]	temperature
X_i	[–]	conversion of component *i*

Sub- and superscripts

abs	[–]	absolute
cat	[–]	catalyst
gas	[–]	gas

Abbreviations

BMBF	German Federal Ministry of Education and Research
BTS	Bayer Technology Service GmbH
CAMERE	carbon dioxide hydrogenation to form methanol via reverse water-gas shift reaction
CCU	carbon capture and urilization
DFT	density functional theory
KEPRI	Korea Electric Power Research Institute
KIT	Karlsruhe Institute of Technology
NRTL	non-random two-liquid
POSCO	Pohang Iron and Steel Company
PtL	power-to-liquid
RWGS	reverse water-gas shift
TRL	technology readiness level
WGS	water-gas shift
wt.	weight

References

[1] D. Kweku, O. Bismark, A. Maxwell, K. Desmond, K. Danso, E. Oti-Mensah, A. Quachie, B. Adormaa, *JSRR* **2018**, *17* (*6*), 1–9. DOI: https://doi.org/10.9734/JSRR/2017/39630

[2] D. B. Botkin, H. Saxe, M. B. Araújo, R. Betts, R. H. W. Bradshaw, T. Cedhagen, P. Chesson, T. P. Dawson, J. R. Etterson, D. P. Faith, et al., *BioScience* **2007**, *57* (*3*), 227–236. DOI: https://doi.org/10.1641/B570306

[3] M. Wei, C. A. McMillan, S. De La Rue Du Can, *Curr. Sustainable Renewable Energy Rep.* **2019**, *6* (*4*), 140–148. DOI: https://doi.org/10.1007/s40518-019-00136-1

[4] P. Gabrielli, L. Rosa, M. Gazzani, R. Meys, A. Bardow, M. Mazzotti, G. Sansavini, *One Earth* **2023**, *6* (*6*), 682–704. DOI: https://doi.org/10.1016/j.oneear.2023.05.006

[5] E. Commission, D.-G. for Communication, *Europäischer Grüner Deal – Die Verwirklichung Unserer Ziele*, Publications Office of the European Union **2021**.

[6] M. Wenzel, *Reverse Water-Gas Shift Chemical Looping for Syngas Production from CO2*, Ph.D. Thesis, Otto-vonGuericke-Universität Magdeburg **2018**.

[7] W. M. Haynes, *CRC Handbook of Chemistry and Physics*, CRC Press, Boca Raton, FL **2014**.

[8] T. Sakakura, J.-C. Choi, H. Yasuda, *Chem. Rev.* **2007**, *107* (*6*), 2365–2387. DOI: https://doi.org/10.1021/cr068357u

[9] P. Voßnacker, A. Wüst, T. Keilhack, C. Müller, S. Steinhauer, H. Beckers, S. Yogendra, Y. Schiesser, R. Weber, M. Reimann, et al., *Sci. Adv.* **2021**, *7* (*40*), eabj5186. DOI: https://doi.org/10.1126/sciadv.abj5186

[10] N. Yoneda, S. Kusano, M. Yasui, P. Pujado, S. Wilcher, *Appl. Catal., A* **2001**, *221* (*1–2*), 253–265. DOI: https://doi.org/10.1016/S0926-860X(01)00800-6

[11] M. Pérez-Fortes, J. C. Schöneberger, A. Boulamanti, E. Tzimas, *Appl. Energy* **2016**, *161*, 718–732. DOI: https://doi.org/10.1016/j.apenergy.2015.07.067

[12] M. Held, D. Schollenberger, S. Sauerschell, S. Bajohr, T. Kolb, *Chem. Ing. Tech.* **2020**, *92* (*5*), 595–602. DOI: https://doi.org/10.1002/cite.201900181

[13] *Elements of Physical Chemistry*, 5th ed. (Eds.: P. W. Atkins, J. De Paula), Oxford University Press, Oxford **2009**.

[14] M. González-Castaño, B. Dorneanu, H. Arellano-García, *React. Chem. Eng.* **2021**, *6* (*6*), 954–976. DOI: https://doi.org/10.1039/D0RE00478B

[15] *Handbook of Heterogeneous Catalysis*, 1st ed. (Eds.: G. Ertl, H. Knözinger, J. Weitkamp), Wiley-VCH Verlag, Weinheim **1997**.

[16] C. Li, X. Yuan, K. Fujimoto, *Appl. Catal., A* **2014**, *469*, 306–311. DOI: https://doi.org/10.1016/j.apcata.2013.10.010

[17] M. B. Fichtl, D. Schlereth, N. Jacobsen, I. Kasatkin, J. Schumann, M. Behrens, R. Schlögl, O. Hinrichsen, *Appl. Catal., A* **2015**, *502*, 262–270. DOI: https://doi.org/10.1016/j.apcata.2015.06.014

[18] H. Ruland, H. Song, D. Laudenschleger, S. Stürmer, S. Schmidt, J. He, K. Kähler, M. Muhler, R. Schlögl, *ChemCatChem* **2020**, *12* (*12*), 3216–3222. DOI: https://doi.org/10.1002/cctc.202000195

[19] T. L. LeValley, A. R. Richard, M. Fan, *Int. J. Hydrogen Energy* **2014**, *39* (*30*), 16983–17000. DOI: https://doi.org/10.1016/j.ijhydene.2014.08.041

[20] *Technische Chemie*, 3rd ed. (Eds.: M. Baerns, A. Behr), Wiley-VCH Verlag, Weinheim **2023**.

[21] B. Smith, J. Muruganadam, L. Murthy, S. Shantha, *Int. J. Chem. React. Eng.* **2010**, *8* (*1*). DOI: https://doi.org/10.2202/1542-6580.2238

[22] L. Wang, W. Chen, D. Zhang, Y. Du, R. Amal, S. Qiao, J. Wu, Z. Yin, *Chem. Soc. Rev.* **2019**, *48* (*21*), 5310–5349. DOI: https://doi.org/10.1039/C9CS00163H

[23] S. N. Habisreutinger, L. Schmidt-Mende, J. K. Stolarczyk, *Angew. Chem., Int. Ed.* **2013**, *52* (*29*), 7372–7408. DOI: https://doi.org/10.1002/anie.201207199

[24] Y. A. Daza, J. N. Kuhn, *RSC Adv.* **2016**, *6* (*55*), 49675–49691. DOI: https://doi.org/10.1039/C6RA05414E

[25] A. Wolf, A. Jess, C. Kern, *Chem. Eng. Technol.* **2016**, *39* (*6*), 1040–1048. DOI: https://doi.org/10.1002/ceat.201500548

[26] S. Adelung, S. Maier, R.-U. Dietrich, *Chem. Ing. Tech.* **2018**, *90* (*9*), 1145–1145. DOI: https://doi.org/10.1002/cite.201855028

[27] *The Properties of Gases and Liquids*, 5. ed. (Eds.: B. E. Poling, J. M. Prausnitz, J. P. O'Connell), McGraw-Hill, New York **2001**.

[28] A. Schmidt, *Technical Thermodynamics for Engineers: Basics and Applications*, Springer International Publishing, Cham **2019**.

[29] A. Münster, *Classical Thermodynamics*, Wiley-Interscience, London **1970**.

[30] D. Rüger, S. Becker, D. Hiller, *Entwicklung der reversen Wassergas-Shift-Reaktion (RWGS) zur Herstellung erneuerbaren Synthesegases für synthetische Flüssigkraftstoffe: Schlussbericht, Laufzeit: 01.07.2016-30.06.2017*, [Sunfire GmbH] **2017**.
[31] C. M. Chun, J. D. Mumford, T. A. Ramanarayanan, *J. Electrochem. Soc.* **2002**, *149* (*7*), B348. DOI: https://doi.org/10.1149/1.1483099
[32] S. Adelung, D. Schnellbögl, R.-U. Dietrich, *Reaktionskinetik der reversen Wassergas-Shift-Reaktion bei Normaldruck zur Übertragung auf die Synthesegasbereitstellung im PtL-Prozess*, **2016**.
[33] von Olshausen, Albrecht, Kolarik, Tietz, Brisse, Glauche, *Jess*, SunFire - Herstellung von Kraftstoffen aus CO_2und H_2O unter Nutzung regenerativer Energie, Sunfire GmbH, **2015**.
[34] hte GmbH the high throughput experimentation company, C. Lizandara, A. Lange de Oliveira, S. A. Schunk, *Feste und fluide Produkte aus Gas - FfPaG: Teil-Schlussbericht hte GmbH*, Hte GmbH; Heidelberg **2017**.
[35] A. Heinzel, T. Haselsteiner, *Verfahren und Vorrichtung zur Erzeugung von Kohlenmonoxid durch reverse Wassergas-Shift, World Intellectual Property Organization WO2021098980A1*, **2021**.
[36] L. Liu, J. Dai, Z. Yang, Y. Li, X. Su, Z. Zhang, *Chem. Eng. J.* **2022**, *431*, 134009. DOI: https://doi.org/10.1016/j.cej.2021.134009
[37] *"enArgus Förderprojekte - Verbundvorhaben: Scoore - Synthesegas aus CO2-Recycling, ein Schlüsselbaustein für eine CO2-neutrale chemische Industrie; Teilvorhaben: Modellgestützte Technologieentwicklung und großtechnischer Verfahrensnachweis,"* https://www.enargus.de/detail/?id=8781807, **2024**.
[38] T. Lunkenbein, F. Girgsdies, T. Kandemir, N. Thomas, M. Behrens, R. Schlögl, E. Frei, *Angew. Chem., Int. Ed.* **2016**, *55* (*41*), 12708–12712. DOI: https://doi.org/10.1002/anie.201603368
[39] C. V. Ovesen, B. S. Clausen, J. Schiøtz, P. Stoltze, H. Topsøe, J. K. Nørskov, *J. Catal.* **1997**, *168* (*2*), 133–142. DOI: https://doi.org/10.1006/jcat.1997.1629
[40] E. A. Olevsky, *Mater. Sci. Eng.: R: Rep.* **1998**, *23* (*2*), 41–100. DOI: https://doi.org/10.1016/S0927-796X(98)00009-6
[41] M. Favaro, H. Xiao, T. Cheng, W. A. Goddard, J. Yano, E. J. Crumlin, *Proc. Natl. Acad. Sci. U.S.A.* **2017**, *114* (*26*), 6706–6711. DOI: https://doi.org/10.1073/pnas.1701405114
[42] X. Chang, T. Wang, J. Gong, *Energy Environ. Sci.* **2016**, *9* (*7*), 2177–2196. DOI: https://doi.org/10.1039/C6EE00383D
[43] S. Fujita, *J. Catal.* **1992**, *134* (*1*), 220–225. DOI: https://doi.org/10.1016/0021-9517(92)90223-5
[44] L.-X. Wang, L. Wang, F.-S. Xiao, *Chem. Sci.* **2021**, *12* (*44*), 14660–14673. DOI: https://doi.org/10.1039/D1SC03109K
[45] J. S. Yoo, F. Abild-Pedersen, J. K. Nørskov, F. Studt, *ACS Catal.* **2014**, *4* (*4*), 1226–1233. DOI: https://doi.org/10.1021/cs400664z
[46] L. Dietz, S. Piccinin, M. Maestri, *J. Phys. Chem. C.* **2015**, *119* (*9*), 4959–4966. DOI: https://doi.org/10.1021/jp512962c
[47] L. C. Grabow, A. A. Gokhale, S. T. Evans, J. A. Dumesic, M. Mavrikakis, *J. Phys. Chem. C.* **2008**, *112* (*12*), 4608–4617. DOI: https://doi.org/10.1021/jp7099702
[48] A. A. Gokhale, J. A. Dumesic, M. Mavrikakis, *J. Am. Chem. Soc.* **2008**, *130* (*4*), 1402–1414. DOI: https://doi.org/10.1021/ja0768237
[49] M. Maestri, K. Reuter, *Chem. Eng. Sci.* **2012**, *74*, 296–299. DOI: https://doi.org/10.1016/j.ces.2012.02.043
[50] A. Donazzi, A. Beretta, G. Groppi, P. Forzatti, *J. Catal.* **2008**, *255* (*2*), 259–268. DOI: https://doi.org/10.1016/j.jcat.2008.02.010
[51] M. Maestri, D. Livio, A. Beretta, G. Groppi, *Ind. Eng. Chem. Res.* **2014**, *53* (*27*), 10914–10928. DOI: https://doi.org/10.1021/ie501570b
[52] Y. Qi, Y.-A. Zhu, D. Chen, *Green Chem. Eng.* **2020**, *1* (*2*), 131–139. DOI: https://doi.org/10.1016/j.gce.2020.10.001
[53] F. C. Meunier, D. Tibiletti, A. Goguet, S. Shekhtman, C. Hardacre, R. Burch, *Catal. Today* **2007**, *126* (*1–2*), 143–147. DOI: https://doi.org/10.1016/j.cattod.2006.10.003
[54] G. Peng, S. J. Sibener, G. C. Schatz, S. T. Ceyer, M. Mavrikakis, *J. Phys. Chem. C* **2012**, *116* (*4*), 3001–3006. DOI: https://doi.org/10.1021/jp210408x
[55] G. Pekridis, K. Kalimeri, N. Kaklidis, E. Vakouftsi, E. F. Iliopoulou, C. Athanasiou, G. E. Marnellos, *Catal. Today* **2007**, *127* (*1–4*), 337–346. DOI: https://doi.org/10.1016/j.cattod.2007.05.026
[56] E. Vesselli, M. Rizzi, L. De Rogatis, X. Ding, A. Baraldi, G. Comelli, L. Savio, L. Vattuone, M. Rocca, P. Fornasiero, et al., *J. Phys. Chem. Lett.* **2010**, *1* (*1*), 402–406. DOI: https://doi.org/10.1021/jz900221c
[57] C.-S. Chen, W.-H. Cheng, S.-S. Lin, *Catal. Lett.* **2000**, *68* (*1*), 45–48. DOI: https://doi.org/10.1023/A:1019071117449
[58] B. Yan, B. Zhao, S. Kattel, Q. Wu, S. Yao, D. Su, J. G. Chen, *J. Catal.* **2019**, *374*, 60–71. DOI: https://doi.org/10.1016/j.jcat.2019.04.036
[59] B. Vollbrecht, *Zur Kinetik der Methanolsynthese an einem technischen Cu/ZnO/Al_2O_3-Katalysator*, Ph.D. Thesis, Docupoint Verlag, Magdeburg **2007**.
[60] Y. Qi, J. Yang, X. Duan, Y.-A. Zhu, D. Chen, A. Holmen, *Catal. Sci. Technol.* **2014**, *4* (*10*), 3534–3543. DOI: https://doi.org/10.1039/C4CY00566J
[61] M. Ojeda, R. Nabar, A. U. Nilekar, A. Ishikawa, M. Mavrikakis, E. Iglesia, *J. Catal.* **2010**, *272* (*2*), 287–297. DOI: https://doi.org/10.1016/j.jcat.2010.04.012
[62] J. L. C. Fajín, J. R. B. Gomes, M. N. D. S. Cordeiro, *J. Phys. Chem. C* **2015**, *119* (*29*), 16537–16551. DOI: https://doi.org/10.1021/acs.jpcc.5b01837
[63] J. E. Whitlow, C. F. Parrish, *AIP Conf. Proc.* **2003**, *654* (*1*), 1116–1123. DOI: https://doi.org/10.1063/1.1541409
[64] F. Bustamante, R. M. Enick, A. V. Cugini, R. P. Killmeyer, B. H. Howard, K. S. Rothenberger, M. V. Ciocco, B. D. Morreale, S. Chattopadhyay, S. Shi, *AIChE J.* **2004**, *50* (*5*), 1028–1041. DOI: https://doi.org/10.1002/aic.10099
[65] S. Adelung, T. Ascher, F. Klein, R.-U. Dietrich, *10th World Congress of Chemical Engineering*, Barcelona **2017**.
[66] M. Juneau, M. Vonglis, J. Hartvigsen, L. Frost, D. Bayerl, M. Dixit, G. Mpourmpakis, J. R. Morse, J. W. Baldwin, H. D. Willauer, et al., *Energy Environ. Sci.* **2020**, *13* (*8*), 2524–2539. DOI: https://doi.org/10.1039/D0EE01457E
[67] A. Ranjbar, A. Irankhah, S. F. Aghamiri, *J. Environ. Chem. Eng.* **2018**, *6* (*4*), 4945–4952. DOI: https://doi.org/10.1016/j.jece.2018.07.032
[68] J. C. Matsubu, V. N. Yang, P. Christopher, *J. Am. Chem. Soc.* **2015**, *137* (*8*), 3076–3084. DOI: https://doi.org/10.1021/ja5128133
[69] J. H. Kwak, L. Kovarik, J. Szanyi, *ACS Catal.* **2013**, *3* (*9*), 2094–2100. DOI: https://doi.org/10.1021/cs4001392
[70] P. Panagiotopoulou, D. I. Kondarides, Xenophon. E. Verykios, *Appl. Catal., B* **2009**, *88* (*3–4*), 470–478. DOI: https://doi.org/10.1016/j.apcatb.2008.10.012
[71] H. C. Wu, Y. C. Chang, J. H. Wu, J. H. Lin, I. K. Lin, C. S. Chen, *Catal. Sci. Technol.* **2015**, *5* (*8*), 4154–4163. DOI: https://doi.org/10.1039/C5CY00667H
[72] J. J. Villora-Picó, J. González-Arias, L. Pastor-Pérez, J. A. Odriozola, T. R. Reina, *Environ. Res.* **2024**, *240*, 117520. DOI: https://doi.org/10.1016/j.envres.2023.117520
[73] P. Ebrahimi, A. Kumar, M. Khraisheh, *emergent mater.* **2020**, *3* (*6*), 881–917. DOI: https://doi.org/10.1007/s42247-020-00116-y

[74] M. Juneau, M. Vonglis, J. Hartvigsen, L. Frost, D. Bayerl, M. Dixit, G. Mpourmpakis, J. R. Morse, J. W. Baldwin, H. D. Willauer, et al., *Energy Environ. Sci.* **2020**, *13* (*8*), 2524–2539. DOI: https://doi.org/10.1039/D0EE01457E

[75] M. D. Porosoff, J. W. Baldwin, X. Peng, G. Mpourmpakis, H. D. Willauer, *ChemSusChem* **2017**, *10* (*11*), 2408–2415. DOI: https://doi.org/10.1002/cssc.201700412

[76] X. Zhang, X. Zhu, L. Lin, S. Yao, M. Zhang, X. Liu, X. Wang, Y.-W. Li, C. Shi, D. Ma, *ACS Catal.* **2017**, *7* (*1*), 912–918. DOI: https://doi.org/10.1021/acscatal.6b02991

[77] J. R. Morse, M. Juneau, J. W. Baldwin, M. D. Porosoff, H. D. Willauer, *J. CO2 Util.* **2020**, *35*, 38–46. DOI: https://doi.org/10.1016/j.jcou.2019.08.024

[78] K. Oshima, T. Shinagawa, Y. Nogami, R. Manabe, S. Ogo, Y. Sekine, *Catal. Today* **2014**, *232*, 27–32. DOI: https://doi.org/10.1016/j.cattod.2013.11.035

[79] B. Dai, G. Zhou, S. Ge, H. Xie, Z. Jiao, G. Zhang, K. Xiong, *Can. J. Chem. Eng.* **2017**, *95* (*4*), 634–642. DOI: https://doi.org/10.1002/cjce.22730

[80] M. Konsolakis, M. Lykaki, S. Stefa, S. A. C. Carabineiro, G. Varvoutis, E. Papista, G. E. Marnellos, *Nanomaterials* **2019**, *9* (*12*), 1739. DOI: https://doi.org/10.3390/nano9121739

[81] S. R. Ede, Z. Luo, *J. Mater. Chem. A* **2021**, *9* (*36*), 20131–20163. DOI: https://doi.org/10.1039/D1TA04032D

[82] C. Álvarez Galván, J. Schumann, M. Behrens, J. L. G. Fierro, R. Schlögl, E. Frei, *Appl. Catal., B* **2016**, *195*, 104–111. DOI: https://doi.org/10.1016/j.apcatb.2016.05.007

[83] R. Burch, R. J. Chappell, S. E. Golunski, *J. Chem. Soc., Faraday Trans. 1.* **1989**, *85* (*10*), 3569–3578. DOI: https://doi.org/10.1039/F19898503569

[84] M. D. Porosoff, J. G. Chen, *J. Catal.* **2013**, *301*, 30–37. DOI: https://doi.org/10.1016/j.jcat.2013.01.022

[85] C. Chen, *Appl. Catal., A* **2004**, *257* (*1*), 97–106. DOI: https://doi.org/10.1016/S0926-860X(03)00637-9

[86] E. Pahija, C. Panaritis, B. Rutherford, M. Couillard, B. Patarachao, J. Shadbahr, F. Bensebaa, G. S. Patience, D. C. Boffito, *J. CO2 Util.* **2022**, *64*, 102155. DOI: https://doi.org/10.1016/j.jcou.2022.102155

[87] L. Chen, D. Wu, C. Wang, M. Ji, Z. Wu, *J. Environ. Chem. Eng.* **2021**, *9* (*3*), 105183. DOI: https://doi.org/10.1016/j.jece.2021.105183

[88] L. Yang, L. Pastor-Pérez, S. Gu, A. Sepúlveda-Escribano, T. R. Reina, *Appl. Catal., B* **2018**, *232*, 464–471. DOI: https://doi.org/10.1016/j.apcatb.2018.03.091

[89] A. G. Kharaji, A. Shariati, M. A. Takassi, *Chin. J. Chem. Eng.* **2013**, *21* (*9*), 1007–1014. DOI: https://doi.org/10.1016/S1004-9541(13)60573-X

[90] J. K. Nørskov, F. Abild-Pedersen, F. Studt, T. Bligaard, *Proc. Natl. Acad. Sci. U.S.A.* **2011**, *108* (*3*), 937–943. DOI: https://doi.org/10.1073/pnas.1006652108

[91] S. Sengupta, A. Jha, P. Shende, R. Maskara, A. K. Das, *J. Environ. Chem. Eng.* **2019**, *7* (*1*), 102911. DOI: https://doi.org/10.1016/j.jece.2019.102911

[92] M. D. Porosoff, X. Yang, J. A. Boscoboinik, J. G. Chen, *Angew. Chem., Int. Ed.* **2014**, *53* (*26*), 6705–6709. DOI: https://doi.org/10.1002/anie.201404109

[93] L. Pastor-Pérez, M. Shah, E. Le Saché, T. Ramirez Reina, *Catalysts* **2018**, *8* (*12*), 608. DOI: https://doi.org/10.3390/catal8120608

[94] B. Liang, H. Duan, X. Su, X. Chen, Y. Huang, X. Chen, J. J. Delgado, T. Zhang, *Catal. Today* **2017**, *281*, 319–326. DOI: https://doi.org/10.1016/j.cattod.2016.02.051

[95] G. Seuser, M. Martinelli, E. S. Garcia, G. F. Upton, M. Ayala, J. Villarreal, Z. Rajabi, D. C. Cronauer, A. J. Kropf, G. Jacobs, *Appl. Catal., A* **2023**, *650*, 119000. DOI: https://doi.org/10.1016/j.apcata.2022.119000

[96] X. Yang, X. Su, X. Chen, H. Duan, B. Liang, Q. Liu, X. Liu, Y. Ren, Y. Huang, T. Zhang, *Appl. Catal., B* **2017**, *216*, 95–105. DOI: https://doi.org/10.1016/j.apcatb.2017.05.067

[97] C.-S. Chen, W.-H. Cheng, S.-S. Lin, *Appl. Catal., A* **2003**, *238* (*1*), 55–67. DOI: https://doi.org/10.1016/S0926-860X(02)00221-1

[98] L. Wang, H. Liu, Y. Chen, R. Zhang, S. Yang, *Chem. Lett.* **2013**, *42* (*7*), 682–683. DOI: https://doi.org/10.1246/cl.130137

[99] L. Pastor-Pérez, F. Baibars, E. Le Sache, H. Arellano-García, S. Gu, T. R. Reina, *J. CO2 Util.* **2017**, *21*, 423–428. DOI: https://doi.org/10.1016/j.jcou.2017.08.009

[100] R. Schlögl, *Angew. Chem., Int. Ed.* **2015**, *54* (*11*), 3465–3520. DOI: https://doi.org/10.1002/anie.201410738

[101] P. Ebrahimi, A. Kumar, M. Khraisheh, *Catalysts* **2022**, *12* (*10*), 1101. DOI: https://doi.org/10.3390/catal12101101

[102] S. S. Kim, H. H. Lee, S. C. Hong, *Appl. Catal., A* **2012**, *423–424*, 100–107. DOI: https://doi.org/10.1016/j.apcata.2012.02.021

[103] F. M. Pinto, V. Y. Suzuki, R. C. Silva, F. A. La Porta, *Front. Mater.* **2019**, *6*, 260. DOI: https://doi.org/10.3389/fmats.2019.00260

[104] F. Esch, S. Fabris, L. Zhou, T. Montini, C. Africh, P. Fornasiero, G. Comelli, R. Rosei, *Science* **2005**, *309* (*5735*), 752–755. DOI: https://doi.org/10.1126/science.1111568

[105] Y. Namai, K.-I. Fukui, Y. Iwasawa, *Catal. Today* **2003**, *85* (*2–4*), 79–91. DOI: https://doi.org/10.1016/S0920-5861(03)00377-8

[106] Y. Zhu, X. Kong, J. Yin, R. You, B. Zhang, H. Zheng, X. Wen, Y. Zhu, Y.-W. Li, *J. Catal.* **2017**, *353*, 315–324. DOI: https://doi.org/10.1016/j.jcat.2017.07.030

[107] D. J. Pettigrew, D. L. Trimm, N. W. Cant, *Catal. Lett.* **1994**, *28* (*2–4*), 313–319. DOI: https://doi.org/10.1007/BF00806061

[108] S. S. Kim, H. H. Lee, S. C. Hong, *Appl. Catal., A* **2012**, *119–120*, 100–108. DOI: https://doi.org/10.1016/j.apcatb.2012.02.023

[109] H. Sakurai, A. Ueda, T. Kobayashi, M. Haruta, *Chem. Commun.* **1997**, *3*, 271–272. DOI: https://doi.org/10.1039/a606192c

[110] T. Inoue, T. Iizuka, K. Tanabe, *Appl. Catal.* **1989**, *46* (*1*), 1–9. DOI: https://doi.org/10.1016/S0166-9834(00)81390-1

[111] Y. Liu, Z. Li, H. Xu, Y. Han, *Catal. Commun.* **2016**, *76*, 1–6. DOI: https://doi.org/10.1016/j.catcom.2015.12.011

[112] L. Wang, H. Liu, Y. Chen, S. Yang, *Int. J. Hydrogen Energy* **2017**, *42* (*6*), 3682–3689. DOI: https://doi.org/10.1016/j.ijhydene.2016.07.048

[113] N. Ishito, K. Hara, K. Nakajima, A. Fukuoka, *J. Energy Chem.* **2016**, *25* (*2*), 306–310. DOI: https://doi.org/10.1016/j.jechem.2015.12.005

[114] A. Trovarelli, *Catal. Rev.* **1996**, *38* (*4*), 439–520. DOI: https://doi.org/10.1080/01614949608006464

[115] R. W. Dorner, D. R. Hardy, F. W. Williams, H. D. Willauer, *Catal. Commun.* **2010**, *11* (*9*), 816–819. DOI: https://doi.org/10.1016/j.catcom.2010.02.024

[116] B. Lu, K. Kawamoto, *Mater. Res. Bull.* **2014**, *53*, 70–78. DOI: https://doi.org/10.1016/j.materresbull.2014.01.043

[117] W. Wang, Y. Zhang, Z. Wang, J. Yan, Q. Ge, C. Liu, *Catal. Today* **2016**, *259*, 402–408. DOI: https://doi.org/10.1016/j.cattod.2015.04.032

[118] H. Kusama, K. K. Bando, K. Okabe, H. Arakawa, *Appl. Catal., A* **2001**, *205* (*1–2*), 285–294. DOI: https://doi.org/10.1016/S0926-860X(00)00576-7

[119] M. R. Gogate, R. J. Davis, *Catal. Commun.* **2010**, *11* (*10*), 901–906. DOI: https://doi.org/10.1016/j.catcom.2010.03.020

[120] S.-C. Yang, S. H. Pang, T. P. Sulmonetti, W.-N. Su, J.-F. Lee, B.-J. Hwang, C. W. Jones, *ACS Catal.* **2018**, *8* (*12*), 12056–12066. DOI: https://doi.org/10.1021/acscatal.8b04219

[121] E. Le Saché, L. Pastor-Pérez, B. J. Haycock, J. J. Villora-Picó, A. Sepúlveda-Escribano, T. R. Reina, *ACS Sustainable Chem. Eng.* **2020**, *8* (*11*), 4614–4622. DOI: https://doi.org/10.1021/acssuschemeng.0c00551
[122] L. Wang, H. Liu, Y. Liu, Y. Chen, S. Yang, *J. Rare Earths.* **2013**, *31* (*6*), 559–564. DOI: https://doi.org/10.1016/S1002-0721(12)60320-2
[123] M. Li, T. H. My Pham, Y. Ko, K. Zhao, L. Zhong, W. Luo, A. Züttel, *ACS Sustainable Chem. Eng.* **2022**, *10* (*4*), 1524–1535. DOI: https://doi.org/10.1021/acssuschemeng.1c06935
[124] R. Einakchi, Metal Nanoparticles over Active Ionic-Conductive Supports for the Reverse Water Gas Shift Reaction, *Masters Dissertation*, Université D'Ottawa **2016**.
[125] F. Vidal Vázquez, P. Pfeifer, J. Lehtonen, P. Piermartini, P. Simell, V. Alopaeus, *Ind. Eng. Chem. Res.* **2017**, *56* (*45*), 13262–13272. DOI: https://doi.org/10.1021/acs.iecr.7b01606
[126] S. S. Kim, K. H. Park, S. C. Hong, *Fuel Process. Technol.* **2013**, *108*, 47–54. DOI: https://doi.org/10.1016/j.fuproc.2012.04.003
[127] P. Ebrahimi, A. Kumar, M. Khraisheh, *Int. J. Hydrogen Energy* **2022**, *47* (*97*), 41259–41267. DOI: https://doi.org/10.1016/j.ijhydene.2021.12.142
[128] P. C. Zonetti, S. Letichevsky, A. B. Gaspar, E. F. Sousa-Aguiar, L. G. Appel, *Appl. Catal., A* **2014**, *475*, 48–54. DOI: https://doi.org/10.1016/j.apcata.2014.01.004
[129] B. Lu, K. Kawamoto, *J. Environ. Chem. Eng.* **2013**, *1* (*3*), 300–309. DOI: https://doi.org/10.1016/j.jece.2013.05.008
[130] C. Ratnasamy, J. P. Wagner, *Catal. Rev.* **2009**, *51* (*3*), 325–440. DOI: https://doi.org/10.1080/01614940903048661
[131] D.-W. Jeong, W.-J. Jang, J.-O. Shim, W.-B. Han, H.-S. Roh, U. H. Jung, W. L. Yoon, *Renewable Energy* **2014**, *65*, 102–107. DOI: https://doi.org/10.1016/j.renene.2013.07.035
[132] Clariant International Ltd, *Clariant Brochure Catalysts and Adsorbents for Syngas* **2017**.
[133] Clariant International Ltd, *Catalysts for Fuel Cells and On-Site Hydrogen Production* **2022**.
[134] D. B. Pal, R. Chand, S. N. Upadhyay, P. K. Mishra, *Renewable Sustainable Energy Rev.* **2018**, *93*, 549–565. DOI: https://doi.org/10.1016/j.rser.2018.05.003
[135] S. Nehlsen, C. Schmid, "Clariant Catalysts powers Ineratec's green fuel production technology," https://www.clariant.com/en/Corporate/News/2020/07/Clariant-Catalysts-powers-Ineratecrsquos-green-fuel-production-technology, **2020**.
[136] Clariant International Ltd, "Carbon Capture & Utilization (CCU) Crossing out emissions with Power-to-X catalysts," https://www.clariant.com/de/Business-Units/Catalysts/Energy-Transition/Carbon-Capture-and-Utilization, **2024**.
[137] S.-H. Lee, K.-T. Lee, *J. Ceram. Process. Res.* **2020**, *21* (*3*), 296–301. DOI: https://doi.org/10.36410/JCPR.2020.21.3.296
[138] I. Fisch, "INERATEC and Clariant: Joined forces for a cleaner future," https://www.ineratec.de/en/en/ineratec-and-clariant-joined-forces-for-a-cleaner-future, **2024**.
[139] R. B. Unde, *Kinetics and Reaction Engineering Aspects of Syngas Production by the Heterogeneously Catalysed Reverse Water Gas Shift Reaction*, Ph.D. Thesis, Universität Bayreuth **2012**.
[140] S. G. Jadhav, P. D. Vaidya, B. M. Bhanage, J. B. Joshi, *Chem. Eng. Res. Des.* **2014**, *92* (*11*), 2557–2567. DOI: https://doi.org/10.1016/j.cherd.2014.03.005
[141] J. Nakamura, J. A. Rodriguez, C. T. Campbell, *J. Phys.: Condens. Matter.* **1989**, *1*, SB149–SB160. DOI: https://doi.org/10.1088/0953-8984/1/SB/026
[142] K. Ernst, *J. Catal.* **1992**, *134* (*1*), 66–74. DOI: https://doi.org/10.1016/0021-9517(92)90210-9
[143] M. J. L. Ginés, A. J. Marchi, C. R. Apesteguía, *Appl. Catal., A* **1997**, *154* (*1*), 155–171. DOI: https://doi.org/10.1016/S0926-860X(96)00369-9
[144] C. S. Chen, J. H. Wu, T. W. Lai, *J. Phys. Chem. C* **2010**, *114* (*35*), 15021–15028. DOI: https://doi.org/10.1021/jp104890c
[145] T. Osaki, N. Narita, T. Horiuchi, T. Sugiyama, H. Masuda, K. Suzuki, *J. Mol. Catal. A: Chem.* **1997**, *125* (*1*), 63–71. DOI: https://doi.org/10.1016/S1381-1169(97)00080-0
[146] F. Ghodoosi, M. R. Khosravi-Nikou, A. Shariati, *Chem. Eng. Technol.* **2017**, *40* (*3*), 598–607. DOI: https://doi.org/10.1002/ceat.201600220
[147] L. Bian, W. Wang, R. Xia, Z. Li, *RSC Adv.* **2016**, *6* (*1*), 677–686. DOI: https://doi.org/10.1039/C5RA19748A
[148] M. González-Castaño, S. Ivanova, T. Ioannides, M. A. Centeno, J. A. Odriozola, *Catal. Sci. Technol.* **2017**, *7* (*7*), 1556–1564. DOI: https://doi.org/10.1039/C6CY02551J
[149] Y. Zhuang, R. Currie, K. B. McAuley, D. S. A. Simakov, *Appl. Catal., A* **2019**, *575*, 74–86. DOI: https://doi.org/10.1016/j.apcata.2019.02.016
[150] K. W. Ting, Z. Maeno, S. M. A. H. Siddiki, K. Shimizu, T. Toyao, *Chem. Lett.* **2021**, *50* (*1*), 158–161. DOI: https://doi.org/10.1246/cl.200692
[151] S.-W. Park, O.-S. Joo, K.-D. Jung, H. Kim, S.-H. Han, *Korean J. Chem. Eng.* **2000**, *17* (*6*), 719–722. DOI: https://doi.org/10.1007/BF02699123
[152] O.-S. Joo, K.-D. Jung, Y. Jung, CAMERE Process for Methanol Synthesis from CO2Hydrogenation, **2004**.
[153] O. S. Joo, Camere Process for Carbon Dioxide Hydrogenation to Form Methanol, **2000**.
[154] S.-W. Park, O.-S. Joo, K.-D. Jung, H. Kim, S.-H. Han, *Appl. Catal., A* **2001**, *211* (*1*), 81–90. DOI: https://doi.org/10.1016/S0926-860X(00)00840-1
[155] R. Dittmeyer, "Synthetic Fuels from CO2 and Renewable Electricity Can Make a Significant Contribution to Achieving CO2-neutral Mobility," https://www.elab.kit.edu/img/Fact%20Sheets/Fact-Sheet-P2L_ENG.pdf, **2025**.
[156] P. Heinzmann, S. Glöser-Chahoud, F. Schultmann, U. Langenmayr, M. Ruppert, W. Fichtner, U. Arnold, N. Dahmen, C. Fuchs, H. Lam, et al., Ergebnisbericht reFuels – Kraftstoffe neu denken, **2023**.
[157] I. Fisch, "INERATEC produces ASTM-conform Sustainable Aviation Fuel (SAF)," https://www.ineratec.de/en/news/ineratec-produces-astm-compliant-sustainable-aviation-fuel-saf, **2024**.
[158] I. Fisch, "Groundbreaking for E-Fuel Production Plant in Frankfurt," https://www.ineratec.de/en/news/groundbreaking-e-fuel-production-plant-frankfurt, **2024**.
[159] Bayer Technology Services, CO2RRECT : Schlussbericht; Berichtszeitraum: 01.10.10 - 30.09.2013, Technische Informationsbibliothek, Universitätsbibliothek, Leverkusen (u.a.) **2014**.
[160] "norsk e-fuel: About us - Let's take on the biggest challenge of our lifetime," https://www.norsk-e-fuel.com/about-us, **2024**.
[161] "norsk e-fuel: Projects - Scaling production to make aviation sustainable," https://www.norsk-e-fuel.com/projects, **2024**.
[162] "norsk e-fuel: Technology - Our technology will change the aviation industry," https://www.norsk-e-fuel.com/technology, **2024**.
[163] "web.archive.org 20.06.2022; norsk e-fuel: Our technology - our technology can change the aviation industry," https://web.archive.org/web/20220520041048/https:/www.norsk-e-fuel.com/technology, **2022**.

[164] "E-fuels: Axens, Paul Wurth (SMS group) and IFPEN sign an agreement for the co-development of the Reverse Water Gas Shift technology," https://www.axens.net/resources-events/news/pr-e-fuels-axens-paul-wurth-sms-group-and-ifpen-sign-agreement-co-development, **2024**.

[165] "Norsk E-Fuel Contracts Paul Wurth (Sms Group) to Carry out a Feed Study Integrating Axens Technologies for the First E-Fuel Plant," https://www.norsk-e-fuel.com/articles/partnership_paulwurth_axens, **2024**.

[166] M. Kern, F. Glenk, D. Klingler, A. Bode, G. Kolios, S. Schunk, G. Wasserschaff, J. Bernnat, B. Zoels, S. Schmidt, et al., Parallel Preparation of Hydrogen, Carbon Monoxide and a Carbon-Comprising Product, US9834440B2, **2017**.

[167] S. Schneider, S. Bajohr, F. Graf, T. Kolb, *Chem. Ing. Tech.* **2020**, *92* (*8*), 1023–1032. DOI: https://doi.org/10.1002/cite.202000021

[168] D. L. Trimm, *Catal. Today.* **1999**, *49* (*1–3*), 3–10. DOI: https://doi.org/10.1016/S0920-5861(98)00401-5

[169] L. An, C. Dong, Y. Yang, J. Zhang, L. He, *Renewable Energy* **2011**, *36* (*3*), 930–935. DOI: https://doi.org/10.1016/j.renene.2010.08.029

[170] S. Schubert, 13th International Colloquium Fuels: Conventional and Future Energy for Automobiles **2021**.

[171] INERATEC GmbH, "INERATEC produziert erstes e-Fuel an Pionieranlage in Frankfurt", https://www.ineratec.de/de/news/ineratec-produziert-erstes-e-fuel-pionieranlage-frankfurt, **2025**.

